TNO report

FEL-96-A015

Speckle reduction in SAR Imagery by various multi-look techniques

TNO Physics and Electronics
Laboratory

Oude Waalsdorperweg 63
PO Box 96864
2509 JG The Hague
The Netherlands

Phone +31 70 326 42 21
Fax +31 70 328 09 61

Date

January 1998

Author(s)

F.P.Ph. de Vries

Classification

Classified by	:	KTZ L. ter Haar
Classification date	:	17 December 1997

Title	:	Ongerubriceerd
Managementuittreksel	:	Ongerubriceerd
Abstract	:	Ongerubriceerd
Report text	:	Ongerubriceerd
Appendix A	:	Ongerubriceerd

19980706 141

Copy no	:	11
No of copies	:	34
No of pages	:	47 (incl appendix, excl RDP & distribution list)
No of appendices	:	1

All information which is classified according to Dutch regulations shall be treated by the
recipient in the same way as classified information of corresponding value in his own
country. No part of this information will be disclosed to any party.

The classification designation Ongerubriceerd is equivalent to Unclassified, Stg.
Confidentieel is equivalent to Confidential and Stg. Geheim is equivalent to Secret.

DTIC QUALITY INSPECTED 1

DISTRIBUTION STATEMENT A

Approved for public release;
Distribution Unlimited

The TNO Physics and Electronics Laboratory is part of
TNO Defence Research which further consists of:

TNO Prins Maurits Laboratory
TNO Human Factors Research Institute

Netherlands Organization for
Applied Scientific Research (TNO)

Managementuittreksel

Titel	:	Speckle reduction in SAR Imagery by various multi-look techniques
Auteur(s)	:	Ir. F.P.Ph. de Vries
Datum	:	januari 1998
Opdrachtnr.	:	A93KM727
IWP-nr.	:	767.2
Rapportnr.	:	FEL-96-A015

SAR beelden bevatten speckle, een type ruis dat ontstaat door de coherente verwerking van radar-echo's van gedistribueerde doelen. De aanwezigheid van deze ruis vermindert de detecteerbaarheid van objecten in het beeld. De mogelijkheid om gedistribueerde doelen te scheiden en te classificeren, vermindert eveneens. Zoals elke ruisvorm kan speckle worden gereduceerd door middelen, het samennemen van een aantal beeldrealisaties van dezelfde scene. Eén van de technieken die kan worden gebruikt is 'multi-look processing'. Hierbij worden de samenstellende beelden, de 'single-look' beelden, gevormd door voor elk beeld een deel van de beschikbare signaalbandbreedte te gebruiken. Elk deel wordt dan verwerkt tot een single-look beeld van dezelfde scene. Het ruisgereduceerde beeld, het multi-look beeld, wordt verkregen door de beelden incoherent, pixel voor pixel, op te tellen.
Het speckle-gereduceerde beeld heeft nu een verbeterde radiometrische resolutie. Echter, omdat de single-look beelden slechts een deel van de beschikbare bandbreedte gebruiken, zal de geometrische resolutie slechter zijn. De verbeterde radiometrische resolutie wordt verkregen ten koste van de geometrische resolutie. De resulterende resoluties worden bepaald door de manier waarop de beschikbare bandbreedte wordt verdeeld en de gebruikte weegfunctie. Het toepassen van weegfuncties verbetert het zijlusgedrag van de corresponderende impulsresponsie, de lekkage, het zich uiten van (sterke) reflecties buiten de doelpositie wordt dan minder. Dit verbeterde 'lekkage'gedrag gaat ten koste van de geometrische resolutie, dat wil zeggen de breedte van de hoofdlus van de puntdoelresponsie neemt toe.
In dit rapport worden een aantal multi-look technieken onderzocht, die zich onderscheiden in de vorm van de weegfunctie, de breedte van de weegfunctie, de combinatie van verschillende weegfuncties en de posities van de weegfuncties ten opzichte van elkaar.
De voor het beoordelen van de technieken benodigde maten worden behandeld. Deze maten zijn: het equivalente aantal beelden, ENL, hetgeen een maat is voor de ruisvermindering, en de vermogenshalfwaardebreedte van de hoofdlus van de puntdoelresponsie, zijnde een maat voor de geometrische resolutie.

Contents

TNO report

1. Introduction

Speckle appears in SAR images due to coherent processing of radar echoes of
distributed target scatterers. Its presence in SAR images reduces the detectability
of objects in the image and also the capability to separate and classify distributed
targets. Noise can be reduced by averaging. One technique which can be used is
multi-look processing. Here the available signal bandwidth is divided in L parts.
Each part is processed yielding a single look image of the same scene.
By adding the looks incoherently pixel by pixel the speckle reduced image is
obtained. The speckle reduced image has an improved radiometric resolution.
However, since the single look images use only part of the available bandwidth,
the geometric resolution will be worse. Improvement of the radiometric resolution
is obtained at the cost of the geometric resolution. The resulting resolutions are
determined by: how the available bandwidth is partioned and the weighting
function used. Using a weighting function improves the sidelobe behaviour of the
corresponding impulse response at the expense of a broadening of the main lobe
and thus a degradation of the geometric resolution, see [3].
In section 2 we introduce the improvement factor ENL, the Equivalent Number of
Looks. The various multi-looking techniques are treated in section 3.

2.   The improvement factor ENL, the Equivalent Number of Looks

The SAR image of an area of distributed targets will show speckle noise. The observed <u>intensity</u> from a pixel follows exponential statistics. The exponential distribution of a single look intensity image is given by

$$p(I) = \frac{1}{2\sigma^2} e^{\frac{-I}{2\sigma^2}}$$

where the mean value

$$m_I = E[I] = 2\sigma^2$$

and the standard deviation is equal to this mean value

$$\sigma_I = E\left[\left(I - \bar{I}\right)^2\right] = 2\sigma^2$$

In the sequel we assume an available processing bandwidth of B_a with corresponding available azimuth integration time T_a.
We further assume a flat azimuth SAR spectrum, see Figure 1. In practice this assumption is not valid since the azimuth spectrum is shaped by the azimuth antenna gain. In satellite SAR the available bandwidth B_a is roughly 0.8 PRF and the edges of the spectral interval coincide with the 3-dB points of the azimuth beam. We also assume that the thermal noise is small compared to the clutter.
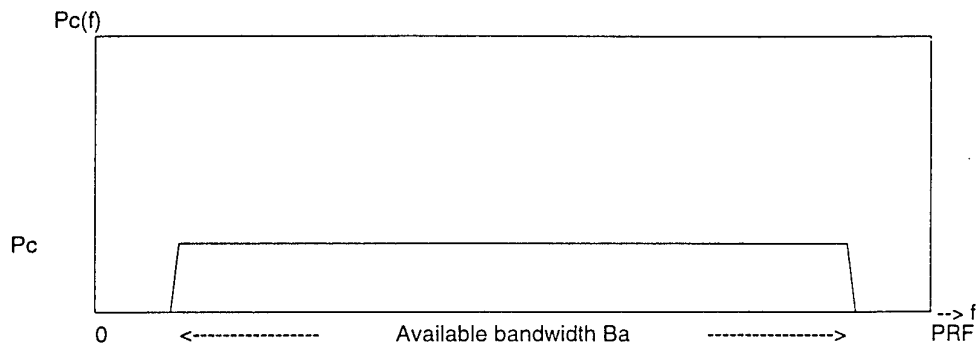
Figure 1:   The azimuth SAR spectrum.

The noise behaviour of single look images is the same, irrespective of their geometric resolution and their spectral position in the available bandwidth (flat spectrum assumption!). To show this, let the mean intensity value of look 1 be m_1 and the variance var_1 and the corresponding values of look 2 m_2 and var_2, then by a simple scaling we can obtain a scaled image with the mean value m_1.

$$m_2' = km_2 = m_1$$

where k is the scaling constant. For the variance of the scaled image we find

$$var_2' = k^2\, var_2$$

with $var_2 = m_2^2$ we have

$$var_2' = k^2 m_2^2 = m_1^2 = var_1$$

Thus the scaled image has the same mean value and variance as the look 1 image.

We now compare the variances of a multi-look image with m_2 and var_2 composed of single look images with m_1 and var_1. The multi-look image is formed so that $m_2 = m_1$. We define the equivalent number of looks (ENL) by

$$var_2 = \frac{1}{ENL}\, var_1$$

Thus $ENL = \dfrac{var_1}{var_2} = \dfrac{m_1^2}{var_2} = \dfrac{m_2^2}{var_2}$

The ENL corresponds to the effective number of statistically independent looks and is given by

$$ENL = \frac{E[I_M]^2}{var[I_M]}$$

where I_M is the intensity of the multi-look image.

In the next chapter we discuss several multi-look techniques where a multi-look intensity image is a weighted sum of single look intensity images.

3.　Multi-look techniques

3.1　Rectangular weighting function, equal looks

The rectangular weighting function is given by

$$w(t) = 1 \qquad -T/2 \leq t \leq T/2$$

Figure 2 shows the weighting function and the corresponding azimuth impulse response profile $g(t_a)$.
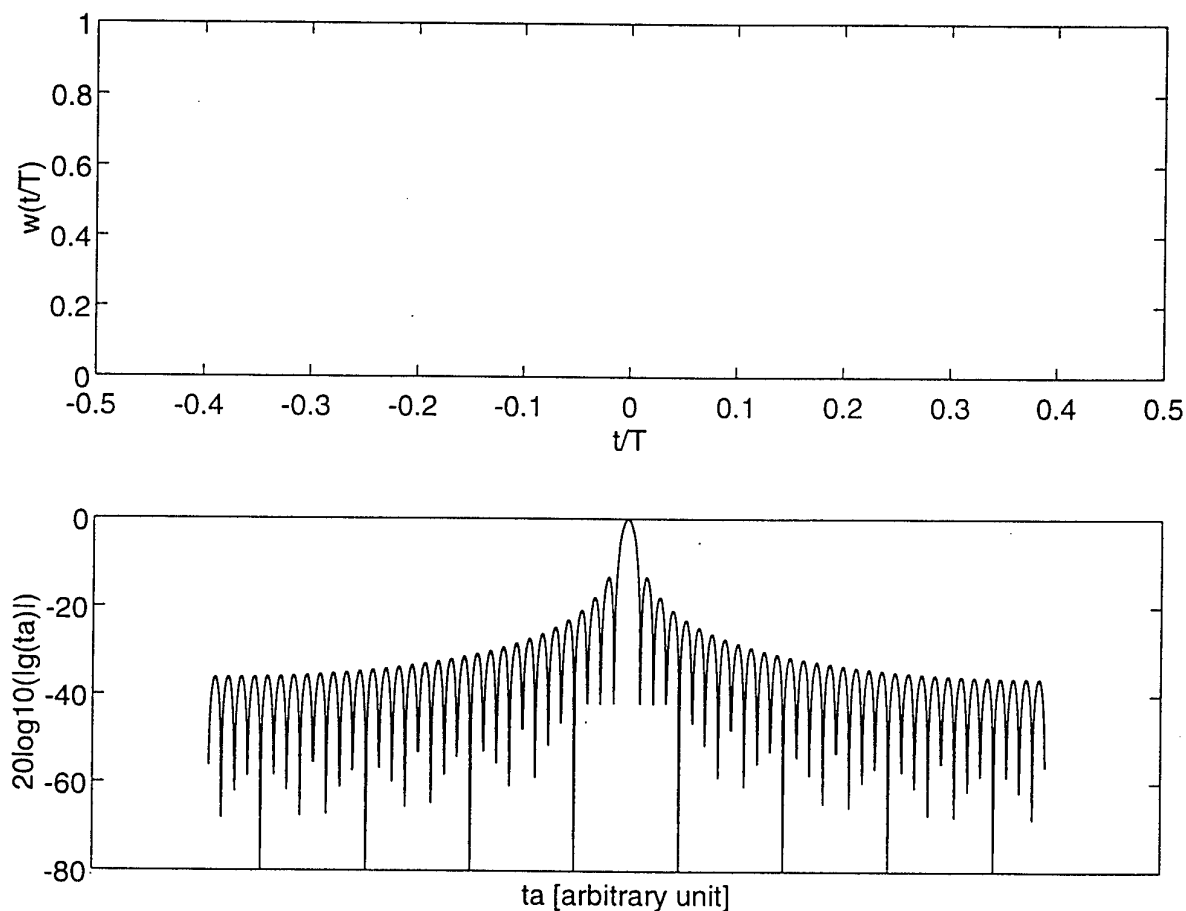
Figure 2:　*The rectangular weighting function and the corresponding azimuth impulse response profile.*

3.1.1　Full resolution image

The full resolution image uses the whole available bandwidth and no weighting function. So the best geometric resolution is obtained. Using the 3-dB resolution measure, the 3-dB bandwidth of the azimuth impulse response is $0.81/B_a$, where B_a is the available bandwidth.

Since no geometrical resolution is sacrificed, no speckle reduction is obtained.

$$ENL = \frac{E[I]}{var[I]} = 1$$

3.1.2   Combination of L_i independent looks

The available integration time is divided into L_i discrete contiguous segments. Each segment is used to generate a lower resolution single look image. The width of each segment is thus $T = \frac{T_a}{L_i}$. The geometrical resolution is reduced by a factor L_i. Thus the 3-dB bandwidth of the azimuth impulse response is $\frac{0.81L_i}{B_a}$.

The mean values and (cross-)variances of the look images are given by $\bar{I}_l = \bar{I}$ for each look image l.

$$\overline{(I_i - \bar{I}_i)(I_j - \bar{I}_j)} \quad = var\, I \quad for\, j = i \quad and$$

$$= 0 \quad for\, j \neq i \qquad (independent\ looks!)$$

The multi-look intensity is given by

$$I_M = \alpha \sum_{l=1}^{L_i} I_l$$

The mean value $\bar{I}_M = \alpha \sum_{l=1}^{L_i} \bar{I}_l = \alpha L_i I$.

The mean value is chosen equal to the single look's mean value, so

$$\alpha L_i = 1$$

The variance follows from

$$\overline{(I_M - \bar{I}_M)^2} = \alpha^2 \overline{\left(\sum_{l=1}^{L_i} (I_l - \bar{I}_l)\right)^2} = \alpha^2 L_i\, var(I)$$

Hence

$$var\, I_M = \frac{var(I)}{L_i}$$

Thus the equivalent number of looks is

$$ENL = \frac{\bar{I}_M^2}{var\, I_M} = L_i$$

Hence the equivalent number of looks is equal to the number of independent looks.

3.1.3   Combination of L overlapping looks

The available integration time is divided into L overlapping segments. The width of each segment corresponds to one of the L_i looks in the independent case (see

3.1.2), $T = T_a/L_j$. The L single-look images are incoherently averaged. The mean values and the (cross-)variances of the look images are given by

$$\bar{I}_l = \bar{I} \text{ for each look image } l.$$

$$\mathrm{var}(I_l) = \overline{\left(I_l - \bar{I}_l\right)^2} = \sigma_l^2 = \sigma^2 \, \mathrm{var}\, I \quad \text{for each look image } l$$

$$\overline{\left(I_i - \bar{I}_i\right)\left(I_j - \bar{I}_j\right)} = \rho_{ij}\sigma_i\sigma_j = \rho_{ij} \, \mathrm{var}\, I$$

where ρ_{ij} is the correlation coefficient between the i-th and j-th look image. The correlation coefficient ρ_{ij} depends on the degree of overlap.

Since all looks have equal weighting, $0 \leq \rho_{ij} \leq 1$ ($\rho_{ij} = 1$, complete overlap and $\rho_{ij} = 0$, complete separation). In appendix A the formula for the correlation coefficient is derived. Figure 3 shows the correlation coefficient as a function of the fractional overlap. As is shown in the appendix, the correlation coefficient

$\rho_{ij} = \rho_{I_i I_j}$ between the intensity images is equal to $\left|\rho_{x_i x_j}\right|^2$, where $\rho_{x_i x_j}$ is the correlation coefficient between the complex valued images x_i and x_j.

The multi-look intensity is given by

$$I_M = \alpha \sum_{l=1}^{L} I_l$$

Proceeding as before we arrive at

$$\bar{I}_M = \bar{I} \ \Rightarrow\ \alpha = \frac{1}{L}$$

$$\mathrm{var}(I_M) = \frac{\displaystyle\sum_{i=1}^{L}\sum_{j=1}^{L}\rho_{ij}}{L^2}\, \mathrm{var}\, I$$

Thus

$$\mathrm{ENL} = \frac{L^2}{\displaystyle\sum_{i=1}^{L}\sum_{j=1}^{L}\rho_{ij}}$$

It turns out that an increase of the ENL is possible, see figure 4.

Since the width of the looks is the same as in case 3.1.2, the geometric resolution is the same.

Rectangular weighting function
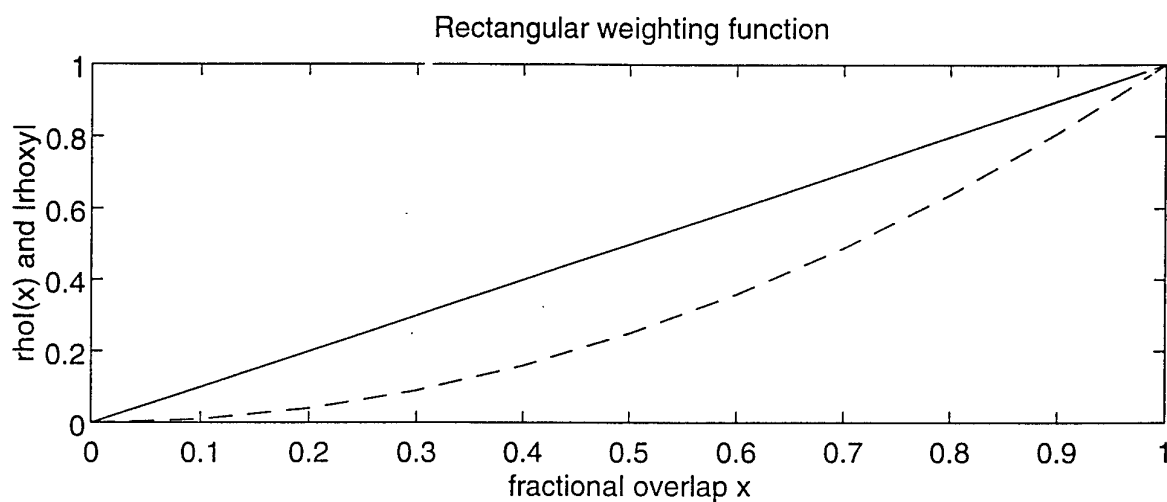
Figure 3:   *The correlation coefficient as a function of the fractional overlap*

    complex images $|\rho_{xy}(x)|$ ——————

    intensity images $\rho_I(x)$ - - - - - - - .

Equivalent Number of looks, Li = 2 and 4, rectangular weighting

Figure 4:   *The ENL as a function of the fractional overlap.*

3.2 Hamming weighting function, equal looks

The Hamming window is a frequently used one (see 3). The function is given by

$$w(t) = \alpha + (1-\alpha)\cos\left(\frac{2\pi}{T}t\right) \qquad -T/2 \le t \le T/2$$

with $\alpha = 0.54$.

The 3-dB bandwidth of the azimuth impulse response profile is $1.30/B_a$.

Figure 5 shows the weighting function and the corresponding azimuth impulse response profile g(t$_a$).
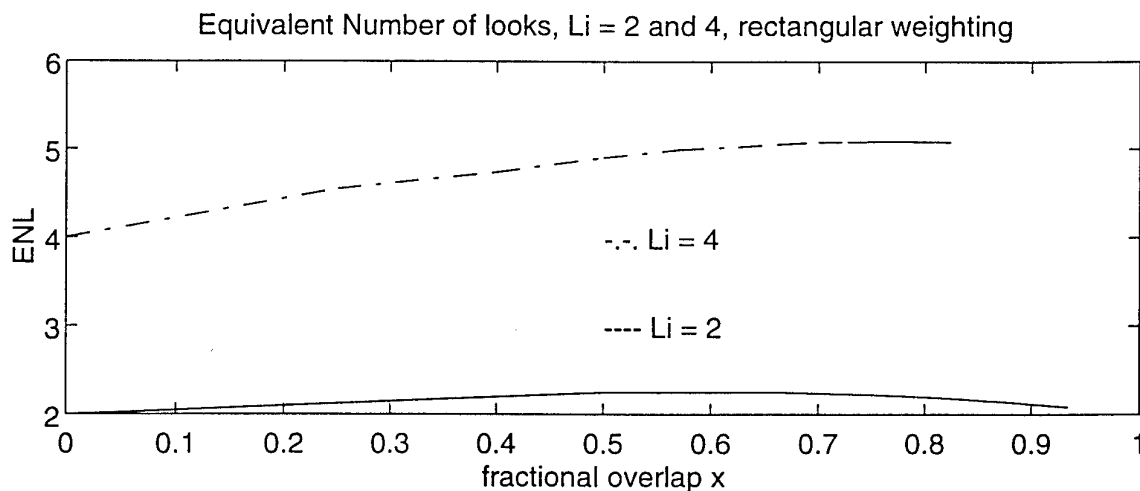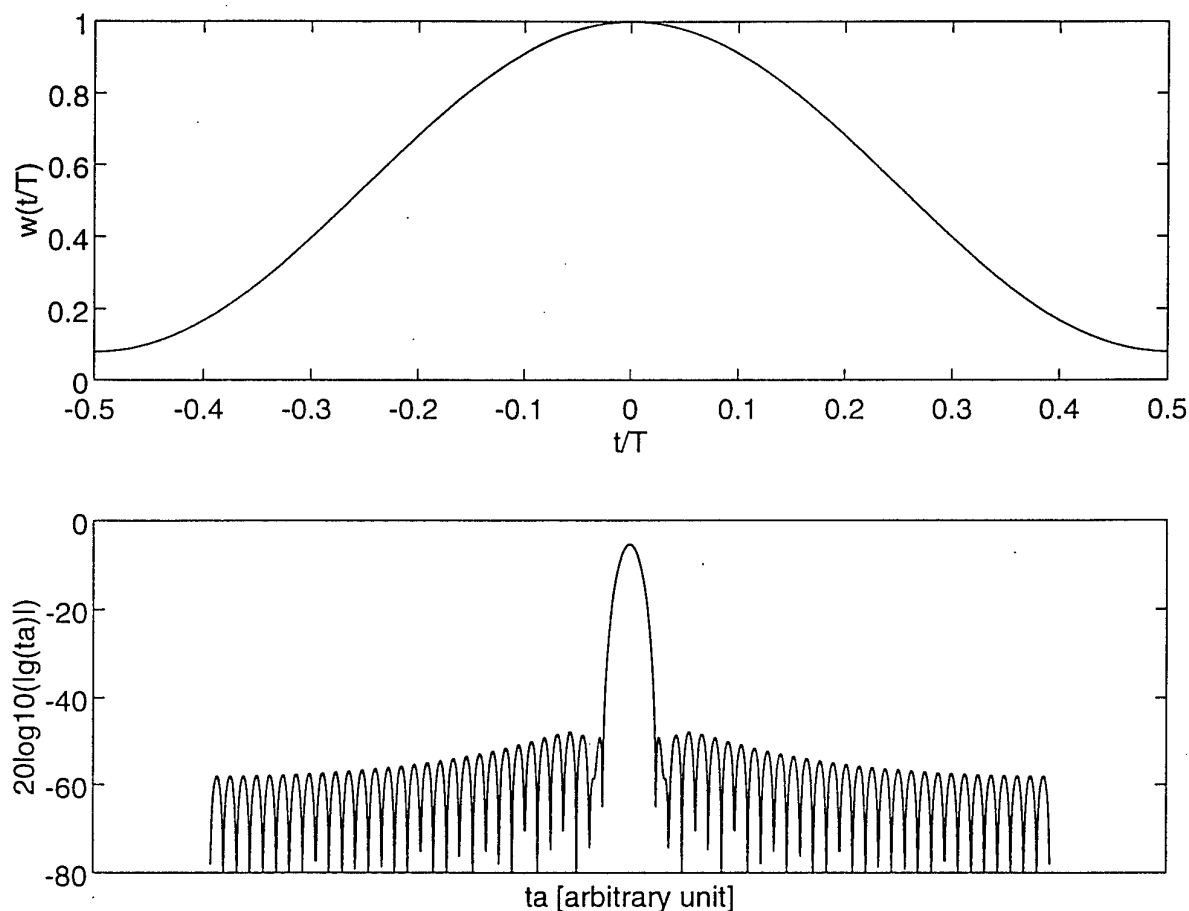

Figure 5:   *The Hamming weighting function and the corresponding azimuth impulse response profile.*

3.2.1   Combination of L$_i$ independent looks

Proceeding as in 3.1.2 we find

The multi-look intensity image is $I_M = \dfrac{1}{L_i} \sum\limits_{l=1}^{L_i} I_l$, the mean value, $\bar{I}_m = \bar{I}$ and the

variance, $\mathrm{var}(I_M) = \dfrac{\mathrm{var}(I)}{L_i}$, thus the ENL $= L_i$.

Comparing this case, the Hamming window, with the results from 3.1.2, the rectangular window, we see that the speckle reduction is the same. However, the geometric resolution is now worse. So, we expect that with Hamming windows a better speckle reduction is attainable. The technique discussed next shows that this is indeed possible.

3.2.2   Combination of L overlapping looks

Proceeding as in 3.1.3 we find
The multi-look intensity image is

$$I_M = \frac{1}{L}\sum_{l=1}^{L} I_l$$

the mean value $\bar{I}_M = \bar{I}$

the variance $var(I_M) = \dfrac{\displaystyle\sum_{i=1}^{L}\sum_{j=1}^{L} \rho_{ij}\, varI}{L^2}$

the Equivalent Number of Looks is $ENL = \dfrac{L^2}{\displaystyle\sum_{i=1}^{L}\sum_{j=1}^{L}\rho_{ij}}$

Figure 6 shows the correlation coefficient as a function of the fractional overlap.
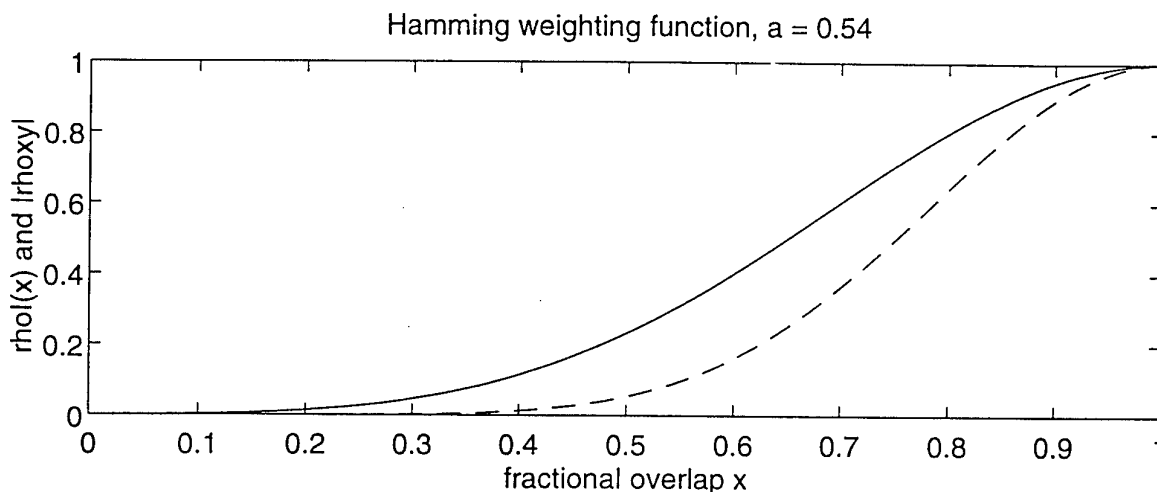
Figure 6:   The correlation coefficient as a function of the fractional overlap:
complex images $|\rho_{xy}(x)|$ ————
intensity images $\rho_I(x)$ - - - - - - - .

As derived in appendix A, $\rho_{ij} = \rho_{I_i I_j} = |\rho_{x_i x_j}|^2$, where $\rho_{I_i I_j}$ is the correlation coefficient of the intensity images and $\rho_{x_i x_j}$ is the correlation coefficient of the complex images.
Comparing the ρ-values from this figure with those of figure 3, we see that the 'Hamming' values are smaller. This means that with the same value of the sum of the correlation values we can have more looks in the Hamming case, thus an increased ENL.

Figure 7 shows the ENL as a function of the (overlapped) looks. In the sequel we refer to this multi-look technique as the traditional technique.

Equivalent Number of looks, Li = 2 and 4, Hamming weighting, a = 0.54

Figure 7:   The ENL as a function of the fractional overlap.

3.3   Hamming weighting function, two types of looks
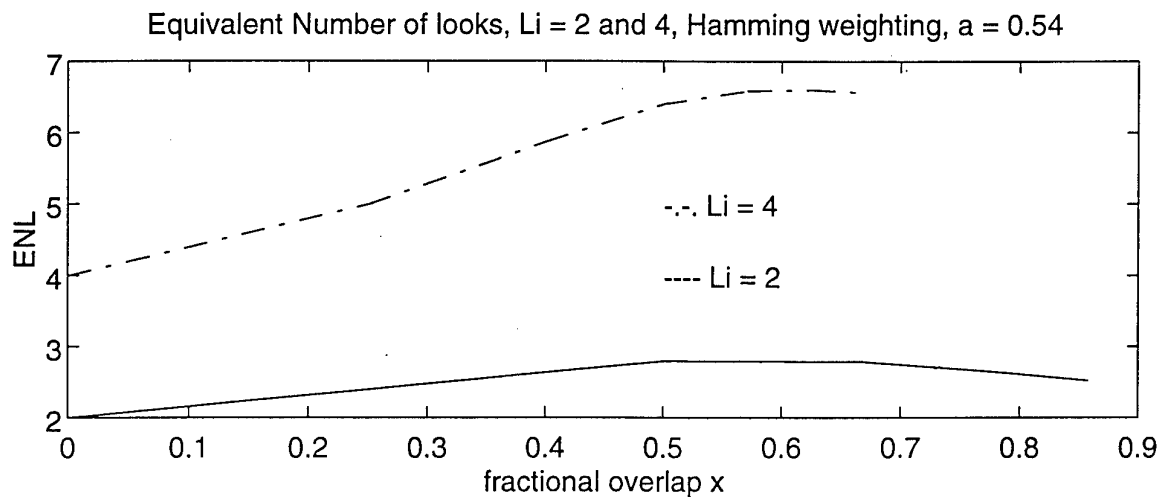
The sections 3.1.3 and 3.2.2 are concerned with overlapping looks, 3.1.3 with looks computed with rectangular weighting functions and 3.2.2 computed with Hamming weighting functions. In both cases an ENL value is obtained larger than the number of independent looks. As explained this originates from the small values of the correlation coefficient values when the overlap is not too large. Since in the Hamming case an inefficient use of the signal spectrum is made by the independent looks, a large number of looks can be inserted with comparably small ρ-values. The 'holes' between the independent looks can profitably be filled with low ρ-value looks. However, the bandwidth at the extremities of the available bandwidth are still not well covered. In reference [1] this is remedied by a technique called the Improved Multi-Look technique (IML-technique). The extreme bandwidth is covered by smaller looks. The time interval length of a small look is the half of the length of a large one. Figure 8 shows how the looks are positioned in the spectral interval. In the next section, we derive the increased ENL and the decreased geometrical resolution.
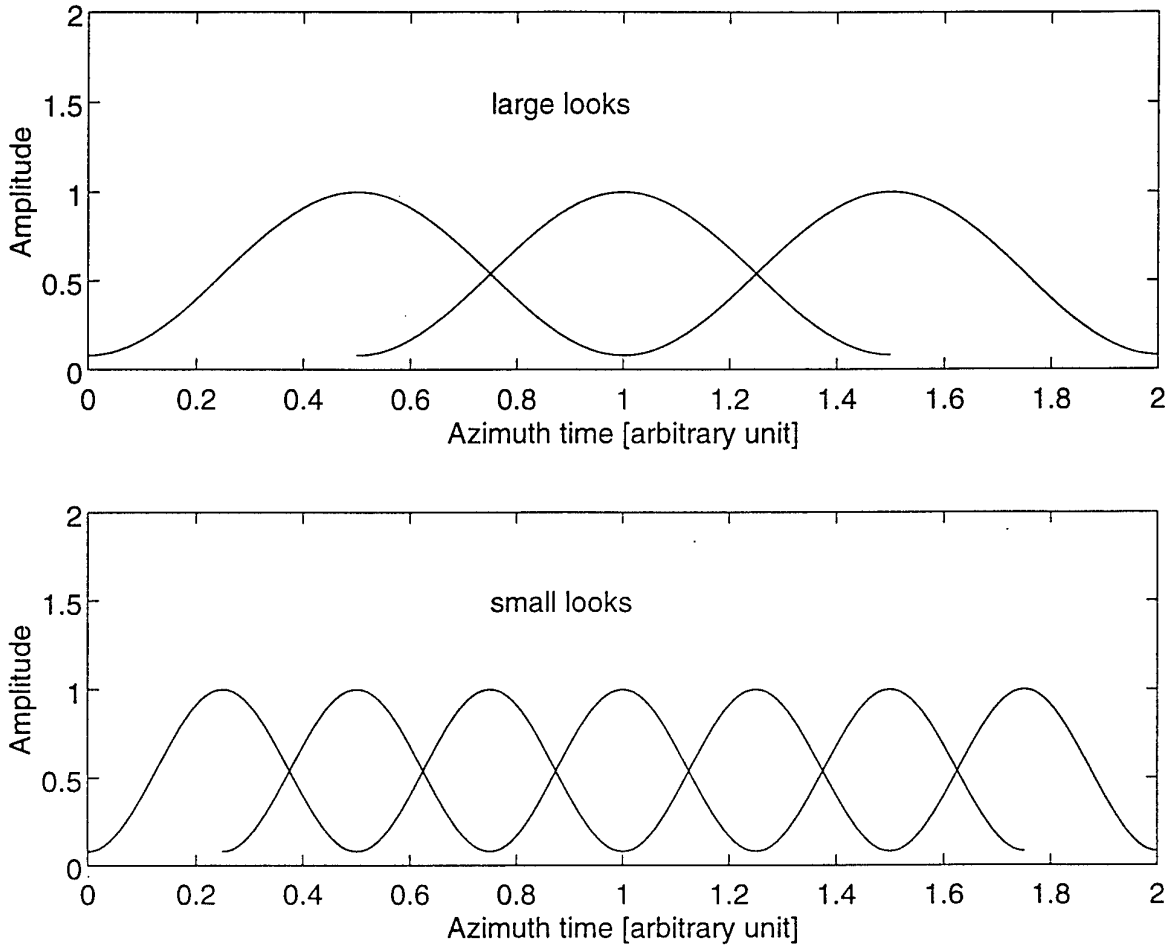
Figure 8:   *Look configuration of the IML technique, $L_i = 2$, overlap = 50%.*

3.3.1 L_L overlapping large looks and L_S overlapping small looks

The mean values and the (cross-)variances of the look images are given by

$$\bar{I}_{L_i} = \bar{I}_L \qquad \text{for } i = 1, 2, \ldots\ldots L_L$$

$$\bar{I}_{s_j} = \bar{I}_S = \bar{I}_L/2 \qquad \text{for } j = 1, 2, \ldots\ldots L_S$$

The (cross-)variances are

$$\overline{\left(I_{L_i} - \bar{I}_{L_i}\right)\left(I_{L_j} - \bar{I}_{L_j}\right)} = \rho_{I_{L_i}I_{L_j}}\sigma_{I_{L_i}}\sigma_{I_{L_j}} = \rho_{I_{L_i}I_{L_j}}\ \text{var}(I_L)$$

$$\overline{\left(I_{L_i} - \bar{I}_{L_i}\right)\left(I_{S_j} - \bar{I}_{S_j}\right)} = \rho_{I_{L_i}I_{S_j}}\sigma_{I_{L_i}}\sigma_{I_{S_j}} = \rho_{I_{L_i}I_{S_j}}\sigma_{I_{L_i}}\frac{\sigma_{I_L}}{2} = \rho_{I_{L_i}I_{L_j}}\frac{\text{var}}{2}(I_L)$$

$$\overline{\left(I_{S_i} - \bar{I}_{S_i}\right)\left(I_{S_j} - \bar{I}_{S_j}\right)} = \rho_{I_{S_i}I_{S_j}}\sigma_{I_{S_i}}\sigma_{I_{S_j}} = \rho_{I_{S_i}I_{S_j}}\frac{\text{var}(I_L)}{4}$$

The multi-look intensity image is

$$I_M = \alpha_L \sum_{i=1}^{L_L} I_{L_i} + \alpha_S \sum_{j=1}^{L_s} I_{Sj}$$

Thus, the mean value

$$\overline{I}_M = \overline{\alpha_L \sum_{i=1}^{L_L} I_{L_i} + \alpha_S \sum_{j=1}^{L_s} I_{Sj}} = \alpha_L \sum_{i=1}^{L_L} \overline{I}_{L_i} + \alpha_S \sum_{j=1}^{L_s} \overline{I}_{Sj} = \alpha_L L_L \overline{I}_L + \alpha_S L_S \frac{\overline{I}_L}{2}$$

This mean value is chosen equal to the mean value of a large look.
Thus

$$\alpha_L L_L \overline{I}_L + \alpha_S L_S \frac{\overline{I}_L}{2} = \overline{I}_L$$

Hence

$$\alpha_L L_L + \frac{\alpha_S L_S}{2} = 1$$

The variance is obtained by

$$var(I_M) = \overline{\left(I_M - \overline{I}_M\right)^2} = \overline{\left\{\alpha_L \sum_{i=1}^{L_L}\left(I_{L_i} - \overline{I}_{L_i}\right) + \alpha_S \sum_{j=1}^{L_s}\left(I_{Sj} - \overline{I}_{Sj}\right)\right\}^2}$$

$$= \alpha_L^2 \sum_{i=1}^{L_L}\sum_{j=1}^{L_L} \sigma_{I_{L_i}}\sigma_{I_{L_j}}\rho_{I_{L_i}I_{L_j}} + 2\alpha_L\alpha_S \sum_{i=1}^{L_L}\sum_{j=1}^{L_s} \sigma_{I_{L_i}}\sigma_{I_{S_j}}\rho_{I_{L_i}I_{S_j}} + \alpha_S^2 \sum_{i=1}^{L_s}\sum_{j=1}^{L_s} \sigma_{I_{S_i}}\sigma_{I_{S_j}}\rho_{I_{S_i}I_{S_j}}$$

$$= var(I_L)\left[\alpha_L^2 \sum_{i=1}^{L_L}\sum_{j=1}^{L_L} \rho_{I_{L_i}I_{L_j}} + \alpha_L\alpha_S \sum_{i=1}^{L_L}\sum_{j=1}^{L_s} \rho_{I_{L_i}I_{S_j}} + \frac{\alpha_S^2}{4} \sum_{i=1}^{L_s}\sum_{j=1}^{L_s} \rho_{I_{S_i}I_{S_j}}\right]$$

Hence

$$ENL = \frac{1}{\left[\alpha_L^2 \sum_{i=1}^{L_L}\sum_{j=1}^{L_L} \rho_{I_{L_i}I_{L_j}} + \alpha_L\alpha_S \sum_{i=1}^{L_L}\sum_{j=1}^{L_s} \rho_{I_{L_i}I_{S_j}} + \frac{\alpha_S^2}{4} \sum_{i=1}^{L_s}\sum_{j=1}^{L_s} \rho_{I_{S_i}I_{S_j}}\right]}$$

The correlation factor $\rho = |\rho_{xy}|$ between two looks is a function of the weighting functions, the look sizes and the overlap. If we use an overlapping of 50% for both the large and the small looks, seven values of ρ can occur (see figure 8).
1. the looks do not overlap, $|\rho_{xy}| = 0$
2. the looks are equal and completely overlap $\rho = 1$
3. the large looks are correlated, ρ_L
4. the small looks are correlated, ρ_S
5. the large look and the small one are weakly correlated ρ_{SL1} (see figure 8, second small look from the left and the second large look from the left)
6. the large look and the small one are correlated ρ_{SL2} (first small and large look)
7. the large look and the small one are strongly correlated ρ_{SL3} (second small look and the first large look from the left).

As explained in appendix A, $\rho_{ij} = \rho_{I_i I_j} = |\rho_{x_i x_j}|^2$

Substituting these values we obtain

$$ENL = \frac{1}{\alpha_L^2\left[L_L + 2(L_L - 1)\rho_L^2\right] + \alpha_L\alpha_s\left[2(L_L - 1)\rho_{SL1}^2 + 2L_L\rho_{SL2}^2 + L_L\rho_{SL3}^2\right] + \frac{\alpha_s^2}{4}\left[L_S + 2(L_S - 1)\rho_s^2\right]}$$

Using the equations from appendix A to calculate the correlation coefficient, we obtain

$\rho_S^2 = 0.0547$, $\rho_L^2 = 0.0547$, $\rho_{SL1}^2 = 0.0062$, $\rho_{SL2}^2 = 0.2693$ and
$\rho_{SL3}^2 = 0.7746$

The number of overlapping looks, given the number of independent looks L_i, is given by

$L_L = 2L_i - 1$
$L_S = 4L_i - 1$
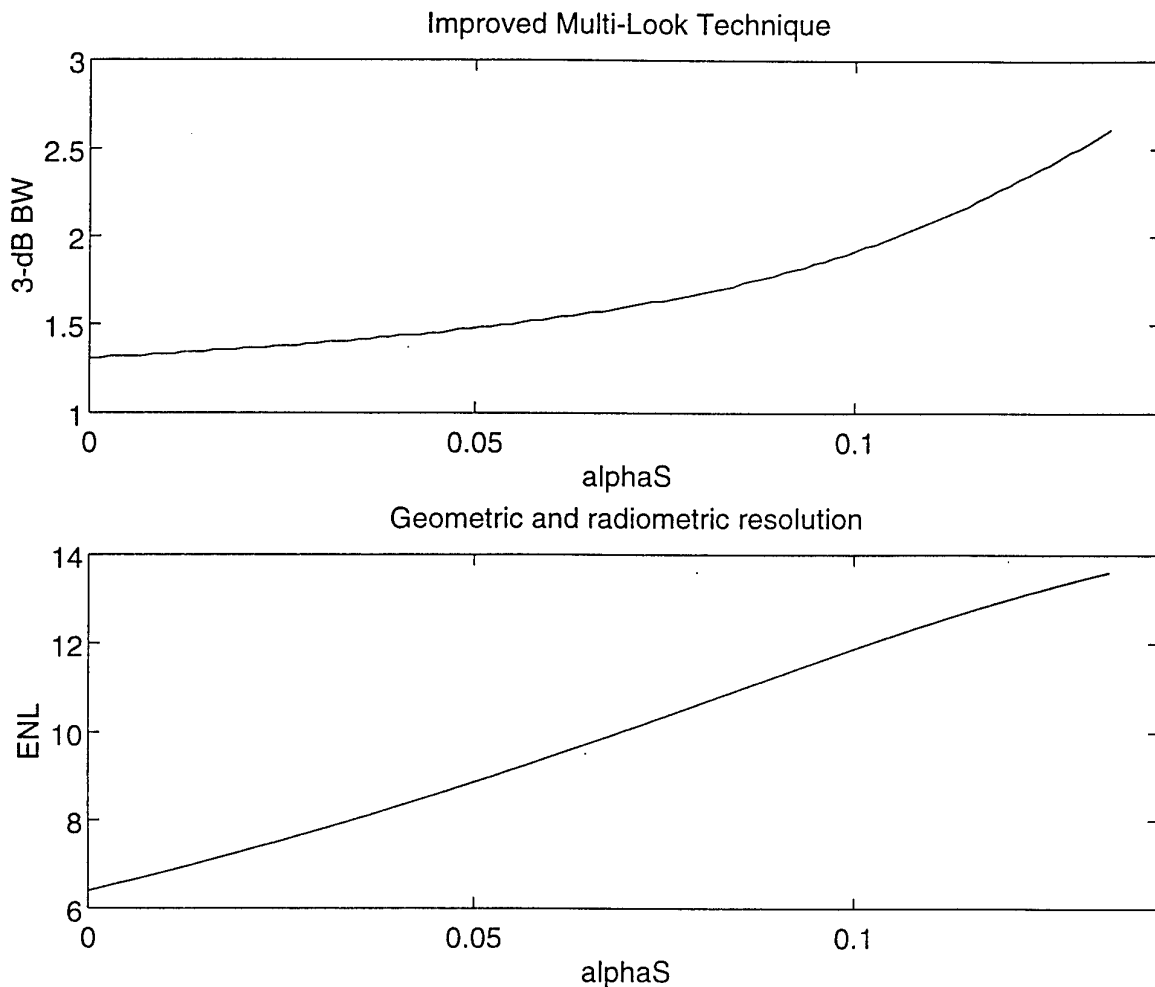
As an example we consider the case for $L_i = 4$.

Figure 9:   The Equivalent Number of Looks and the 3-dB resolution as a function of α_S.

As shown by figure 9, increasing the value of α_S leads indeed to an increase of the ENL and a decrease of the 3-dB BW.

However, this result is predictable as higher α_S values correspond with an increasing relative contribution of the small looks, that is looks with a lower geometric resolution and we know that geometric resolution can be traded for radiometric resolution. For $\alpha_S = 0$ we have the result of section 3.2.2 with $L_i = 4$ (3-dB BW =1.30/Ba). For the other extreme α_S value, corresponding to $\alpha_L = 0$, we have the result of section 3.2.2 with $L_i = 8$ (3-dB BW = 2×1.30/B$_a$).

As a matter of fact, the technique offers to trade radiometric and geometric resolution in a continuous way via the parameter α_S.

The technique fills the 'spectral dips' both in the middle part of the spectral range and at the extremities. The filling at the extremes sets this technique apart from other techniques. In order to prove the favourable effect of filling the edges, we compare the technique with one that fills the middle part in an optimum way. The latter technique uses looks each having the same size T (and Hamming weighting function). The available bandwidth is completely filled with L overlapping looks. The number of looks is taken such that the maximum ENL occurs. Both techniques yield the same geometrical resolution; this is done by choosing the corresponding values of α_S and T. The comparison procedure is
- chose α_S this yields the ENL$_{IML}$ (α_S) and 3-dB BW (α_S)
- take the corresponding 3-dB BW (α_S) value to determine the Hamming window size T(α_S)
- compute the optimum L value for this window, that is the value of L that yields the maximum ENL$_{trad}$.

The results are shown in figure 10. From this figure we see that for almost all values α_S the IML technique yields a higher ENL value. The exceptions are near the edges because there the techniques are equal (they use the same window size T), except for the overlap which is optimum for the traditional technique and 50% for the IML technique.

The quotient $\dfrac{ENL_{IML}}{ENL_{trad}}$ reaches a maximum for $\alpha_S = 0.08$.

Figure 14 also shows that for the same geometrical resolution the IML technique performs better than the traditional.

Figures 11a and 11b show the azimuth impulse response of the IML technique for three values of α_S. The value $\alpha_S = 0$ yields the result of a single look image with $L_i = 4$. The other extreme value ($\alpha_L = 0$) yields the results of a single look image with $L_i = 8$. The bottom curve shows the result for $\alpha_S = 0.08$. This result is especially interesting in that it shows the relative meaning of the geometric resolution measure in this case. Looking at the main lobe we see that only the upper part has the character of a lobe of a single look with the same 3-dB value. The bottom part corresponds with the lower geometrical resolution of the smaller look.
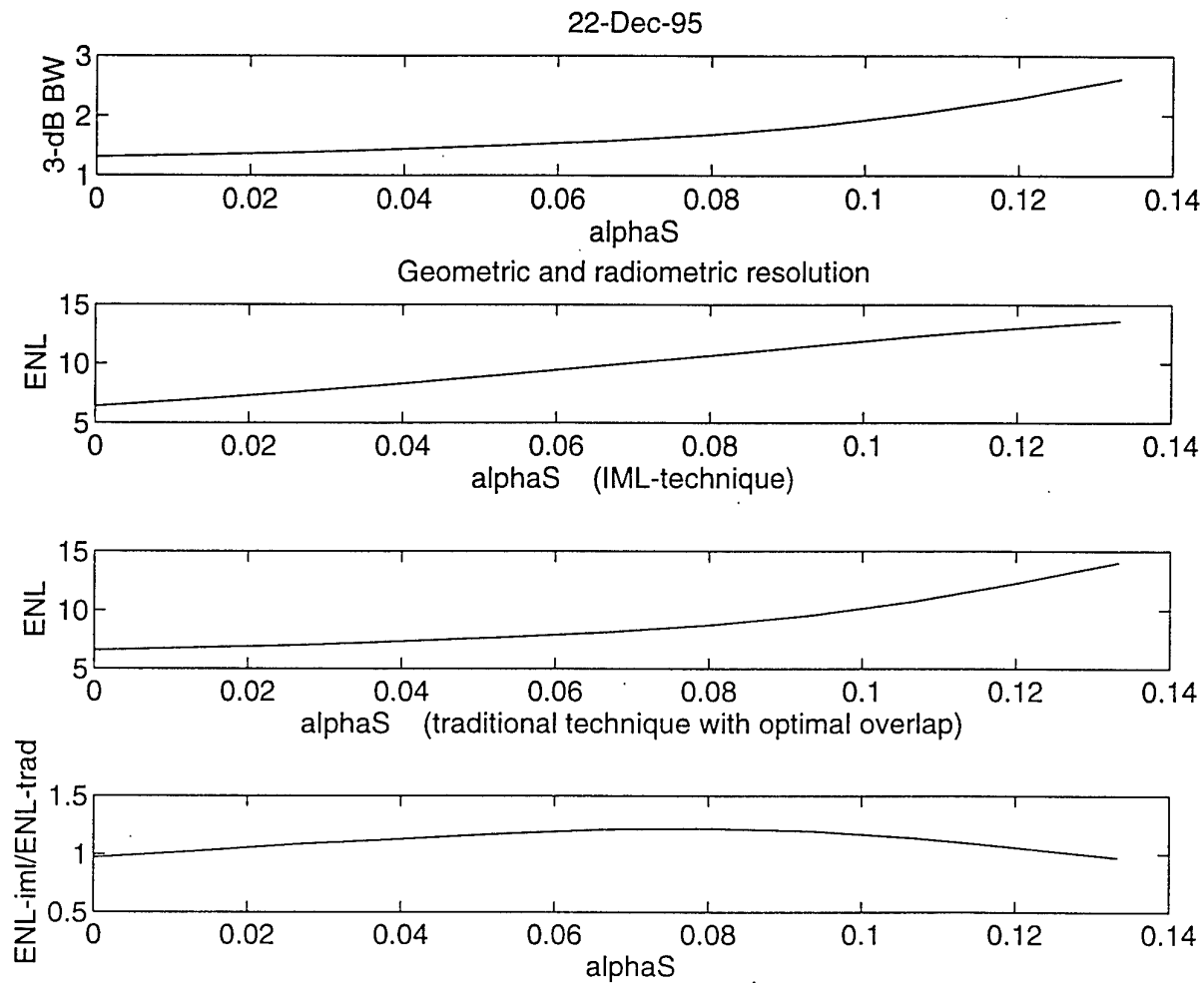
Figure 10: Comparison of the IML and traditional technique with optimum overlap.

Azimuth impulse response of multilook I=aL*sum of 7 looks IL + aS*sum of 15 looks IS

time arbitrary unit -> aL = 0.1429 aS = 0 3-dB BW = 1.3125 / TL

time arbitrary unit -> aL = 0 aS = 0.1333 3-dB BW = 2.6875 / TL

time arbitrary unit -> aL = 0.0571 aS = 0.08 3-dB BW = 1.6875 / TL

Figure 11a: Azimuth impulse response of the IML technique for several values of α_S, logarithmic scale.

Azimuth impulse response of multilook I=aL*sum of 7 looks IL + aS*sum of 15 looks IS
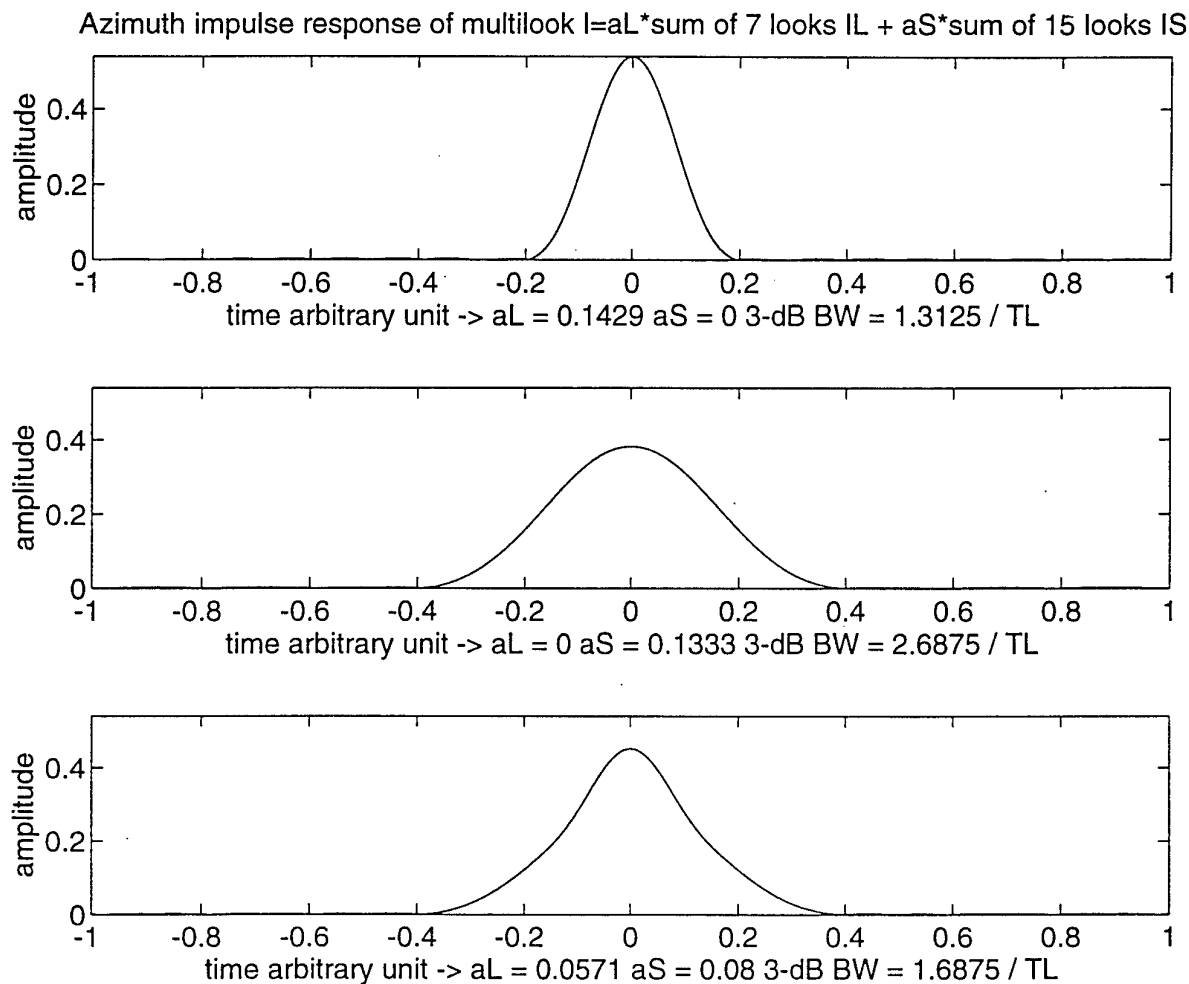
Figure 11b: Azimuth impulse response of the IML technique for several values of α_S, linear scale.

3.3.2 L_L overlapping large looks and 2 small looks

Figure 12 shows the configuration of the technique. Comparing with figure 8 from the IML technique in section 3.3.1, we see that the small looks in the middle part of the available bandwidth are absent. The idea is that the radiome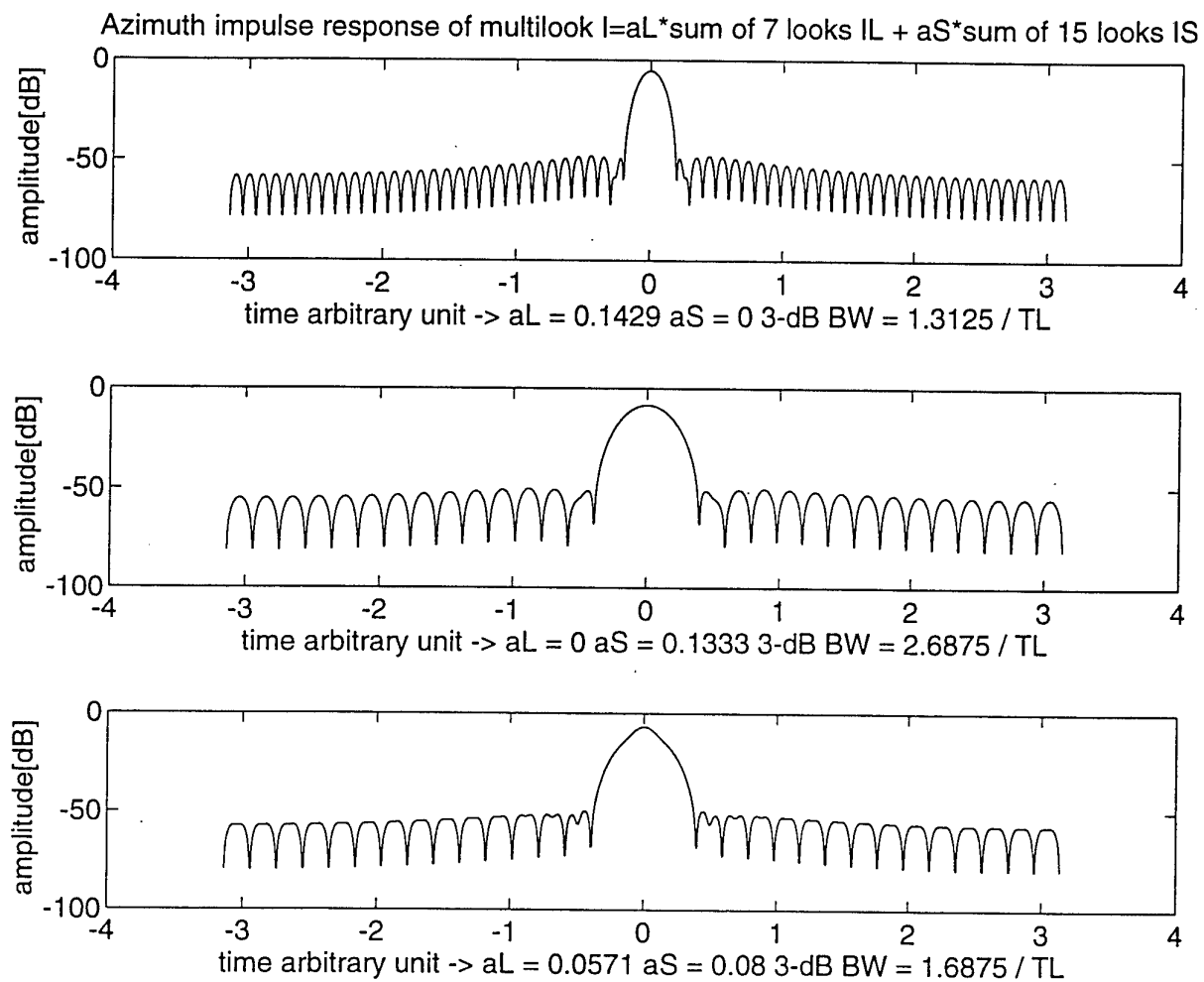tric resolution is improved by the two edge looks but that the geometrical resolution deteriorates less because of the small number of small looks.

The mean values and the (cross-)variances of the look images are given by

$$\bar{I}_{L_i} = \bar{I}_L \qquad \text{for } i = 1, 2, \ldots\ldots L_L$$

$$\bar{I}_{s_j} = \bar{I}_s = \frac{I_L}{2} \qquad \text{for } j = 1, 2$$

The cross variances are

$$\overline{\left(I_{L_i}-\bar{I}_{L_i}\right)\left(I_{L_j}-\bar{I}_{L_j}\right)} = \rho_{I_{L_i}I_{L_j}}\sigma_{I_{L_i}}\sigma_{I_{L_j}} = \rho_{I_{L_i}I_{L_j}}\,\mathrm{var}\left(I_L\right)$$

$$\overline{\left(I_{L_i}-\bar{I}_{L_i}\right)\left(I_{S_j}-\bar{I}_{S_j}\right)} = \rho_{I_{L_i}I_{S_j}}\sigma_{I_{L_i}}\sigma_{I_{S_j}} = \rho_{I_{L_i}I_{S_j}}\sigma_{I_L}\frac{\sigma_{I_L}}{2} = \rho_{I_{L_i}I_{S_j}}\frac{\mathrm{var}\left(I_L\right)}{2}$$

$$\overline{\left(I_{S_i}-\bar{I}_{S_i}\right)\left(I_{S_j}-\bar{I}_{S_j}\right)} = 0 \text{ for } i \neq j$$

$$= \sigma_{I_{S_i}}\sigma_{I_{S_j}} = \frac{\sigma_{I_L}^2}{4} = \mathrm{var}\left(I_L\right) \text{ for } i = j$$

Proceeding as in section 3.3.1 we arrive at

$$\bar{I}_M = \bar{I}_L$$

$$\alpha_L L_L + \frac{\alpha_S L_S}{2} = 1$$

and

$$\mathrm{ENL} = \frac{1}{\alpha_L^2 \sum\limits_{i=1}^{L_L}\sum\limits_{j=1}^{L_L}\rho_{I_{L_i}I_{L_j}} + \alpha_L\alpha_S \sum\limits_{i=1}^{L_L}\sum\limits_{j=1}^{L_L}\rho_{I_{L_i}I_{S_j}} + \frac{\alpha_S^2}{4}\sum\limits_{i=1}^{L_S}\sum\limits_{j=1}^{L_S}\rho_{I_{S_i}I_{S_j}}}$$

As an example we consider the case for overlap = 50%, number of independent looks $L_i = 4$, $L_L = 2L_i\text{-}1$, $L_S = 2$.
Figure 13 shows the ENL and 3-dB BW as a function of α_S, compare this figure with figure 9. Figure 14 shows the ENL as a function of the 3-dB BW; also shown are the curves of the traditional and IML technique.
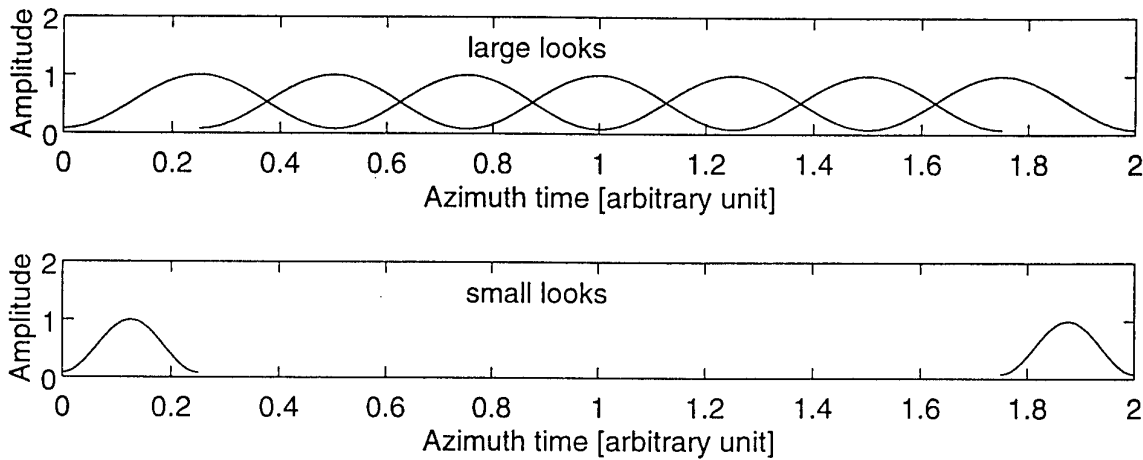

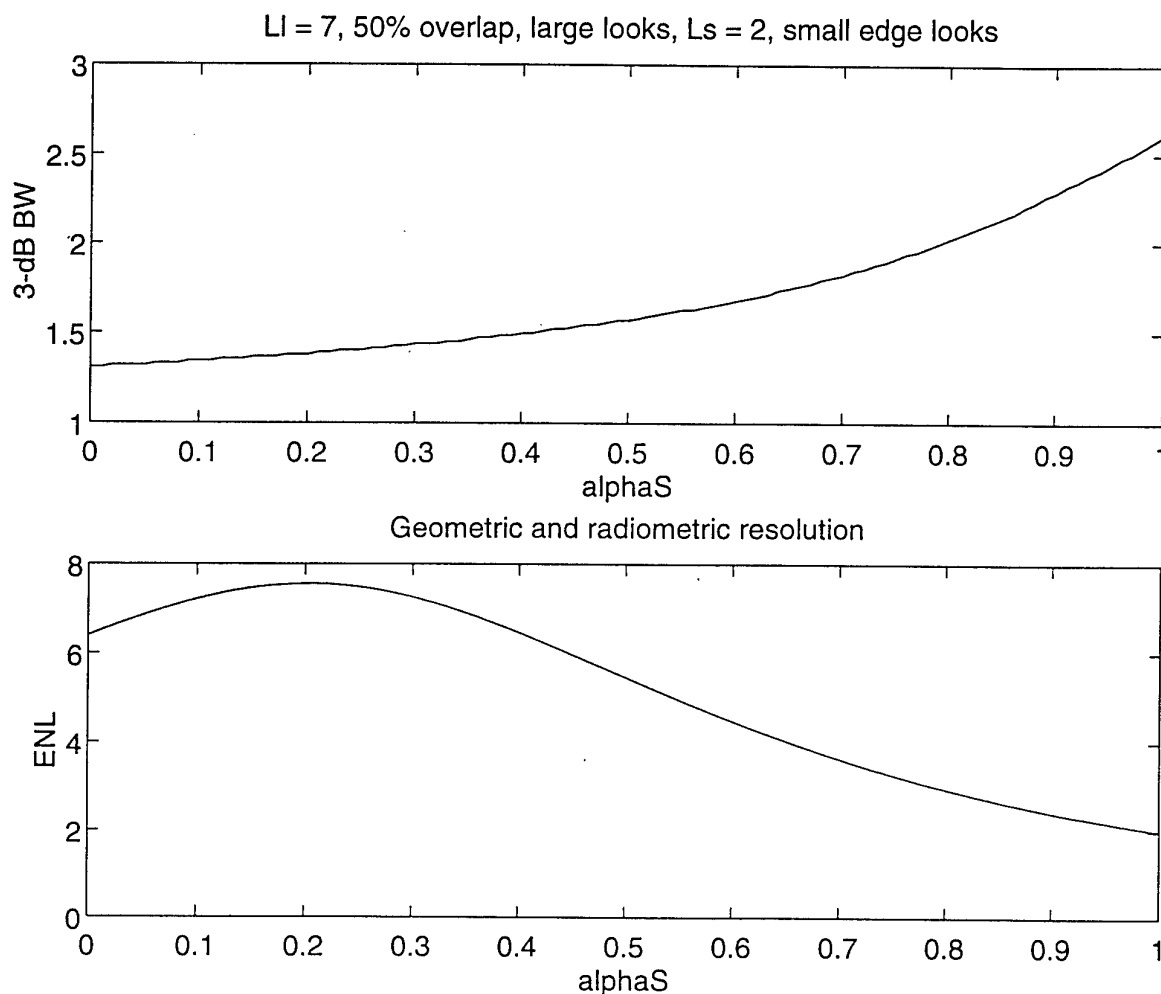*Figure 12: Look configuration of the technique, $L_i = 4$, 50% overlap.*

LI = 7, 50% overlap, large looks, Ls = 2, small edge looks

Geometric and radiometric resolution

Figure 13:   *The Equivalent Number of Looks and the 3-dB resolution as a function of* α_S.

From this figure it can be concluded that this multi-look technique is not appreciably better than the IML technique. Only for the lower values it is slightly better and for the most part it is unusable. Note that in the 3-dB BW range, where it performs almost equally well as the IML technique, it does so in a far more efficient way, only 9 looks have to be computed compared with 22 in the IML case.

Figures 15a and 15b show the azimuth impulse response of the technique for three values of α_S. The value $\alpha_S = 0$ yields the result of a single look image with $T = T_a/4$. The other extreme value ($\alpha_L = 0$) yields the result of a single look image with $T = T_a/8$. The bottom curve shows the result for $\alpha_S = 0.2$ which corresponds with the maximum ENL value attainable. This curve shows, as its corresponding IML curve in figures 11a/b, the relative meaning of the geometric resolution measure in this case. Observing the main lobe, we see that only the upper part has the character of a lobe of a single look with the same 3-dB BW value. The bottom part corresponds with the lower geometrical resolution of the smaller look.

Comparison of multi-look techniques
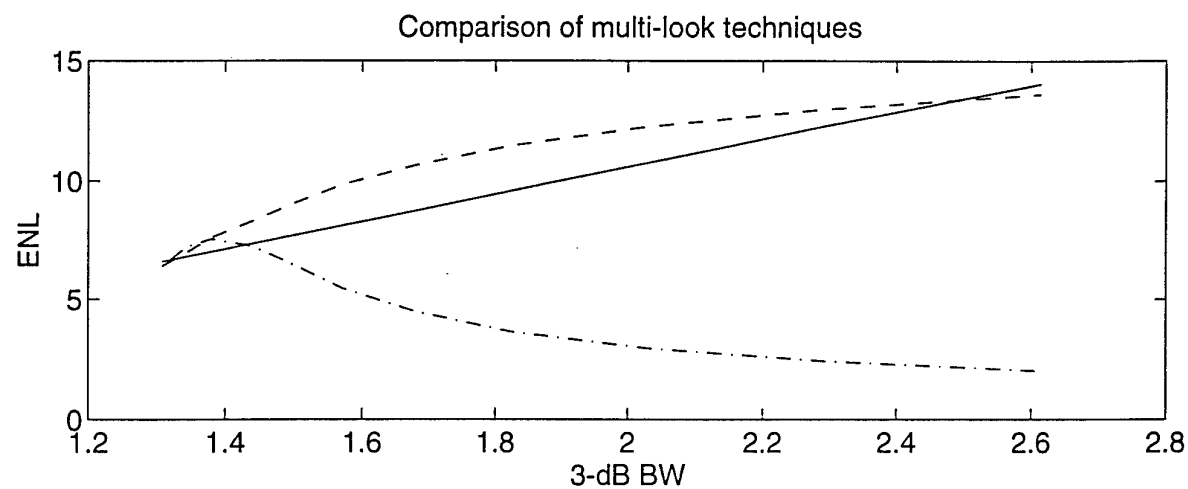
Figure 14:   *ENL as a function of the 3-dB BW for*
             ————— *traditional multi-look technique*
     - - - - - - - *IML technique*
     - · - · - · - *L = 7 S = 2 technique, see section 3.3.2.*

Azimuth impulse response of multilook I=aL*sum of 7 looks IL + aS*sum of 2 looks IS

time arbitrary unit -> aL = 0.1429 aS = 0 3-dB BW = 1.3125 / TL

time arbitrary unit -> aL = 0 aS = 1 3-dB BW = 2.6875 / TL

time arbitrary unit -> aL = 0.1143 aS = 0.2 3-dB BW = 1.3793 / TL

Figure 15a: Azimuth impulse response of the L7S2 multi-look technique for several values of α_S, logarithmic scale.

Azimuth impulse response of multilook I=aL*sum of 7 looks IL + aS*sum of 2 looks IS
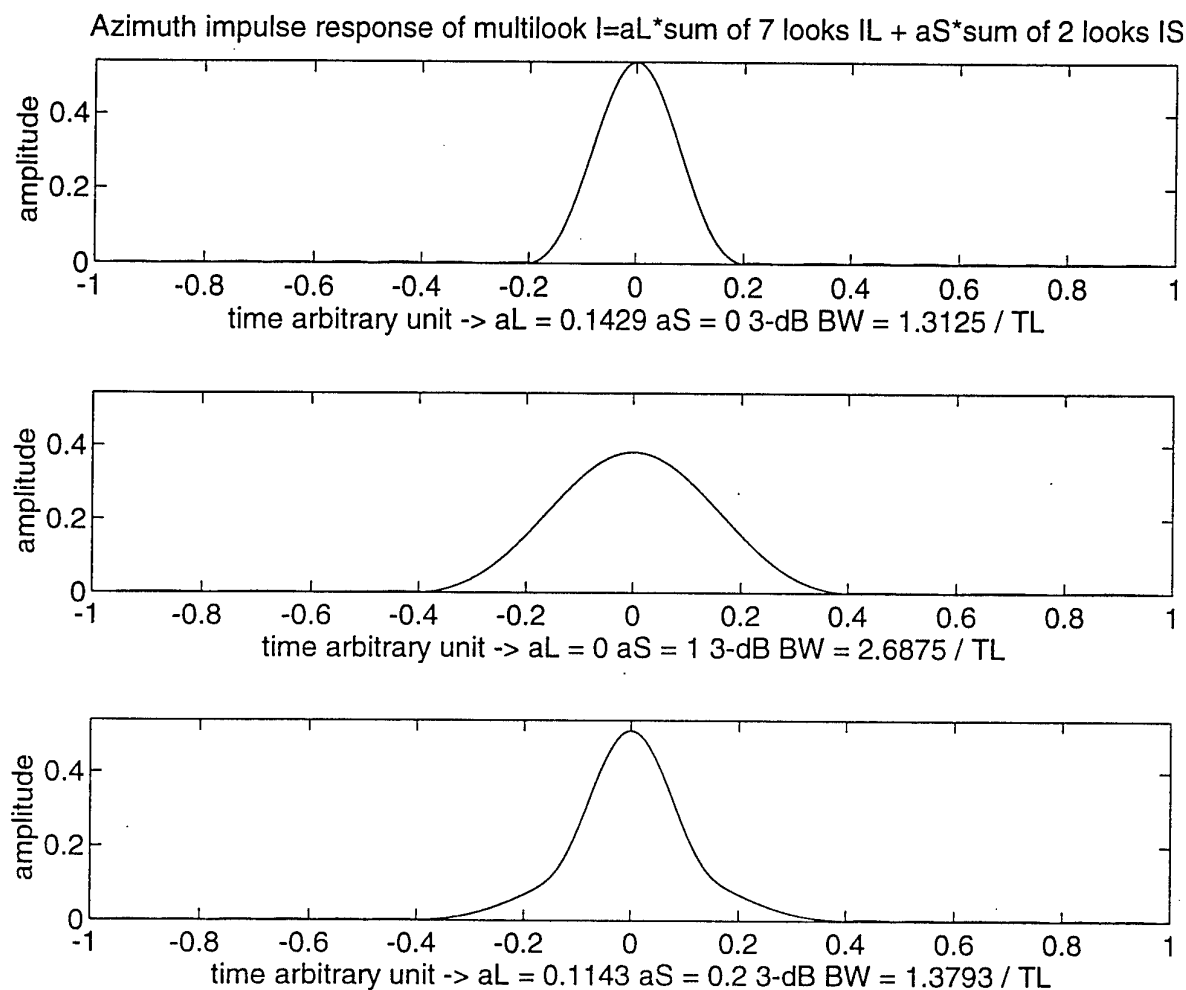
Figure 15b: Azimuth impulse response of the L7S2 multi-look technique for several values of α_S, linear scale.

3.4   Two types of looks, different in weighting function and look size

3.4.1 L_L overlapping large looks and L_S overlapping small looks

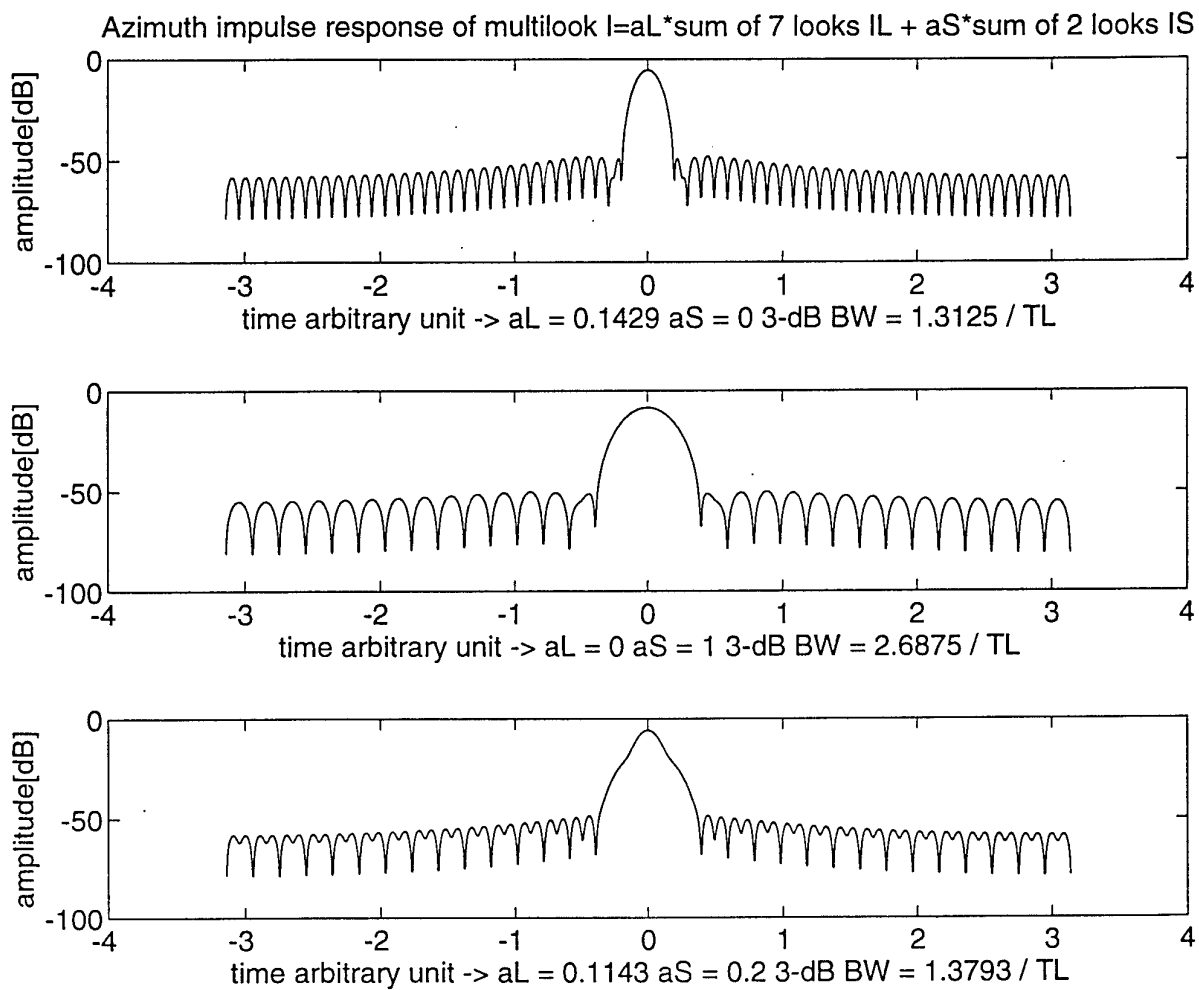We proceed along the same lines as in section 3.3.1. The only difference being the mean value intensity of the small look. In 3.3.1 we considered the case where both weighting functions are Hamming ones and the look size of the small look is one half of that of the large look, thus $\bar{I}_S = \bar{I}_L / 2$. In the general case the number 2 has to be replaced by another number, here called β_m, the value we derive below. The mean intensity value is

$$\bar{I} = P_c \int_{-T/2}^{T/2} w^2(t)\, dt$$

where

P_c is the clutter power spectral density

$w(t)$ is the weighting function and

T is the length of the weighting function.

Evaluating the mean values give

$$\bar{I}_R = P_c T_R \text{ and } \bar{I}_H = 0.375 \, P_c T_H$$

for the rectangular and Hamming windows respectively.

Thus

$$\beta_m = \frac{\bar{I}_L}{\bar{I}_S} = \frac{\bar{I}_H}{\bar{I}_R} = 0.3974 \frac{T_H}{T_R}$$

For the resolution holds

$$B_R = \frac{k_R}{T_R} \text{ and } B_H = \frac{k_H}{T_H}$$

with $\dfrac{k_R}{k_H} = \dfrac{0.89}{1.30}$, see ref [3] table I.

Requiring equal resolution, $B_R = B_H$, we find $T_R = \dfrac{k_R}{k_H} T_H = 0.685 T_H$ and

$$\beta_m = 0.581.$$

The mean values and the (cross-)variances of the look images are given by

$$\bar{I}_{L_i} = \bar{I}_L \qquad \text{for } i = 1, 2, \ldots\ldots L_L$$

$$\bar{I}_{S_j} = \bar{I}_S = \bar{I}_L / \beta_m \qquad \text{for } j = 1, 2, \ldots\ldots L_S$$

The (cross-)variances are

$$\overline{\left(I_{L_i} - \bar{I}_{L_i}\right)\left(I_{L_j} - \bar{I}_{L_j}\right)} = \rho_{I_{L_i} I_{L_j}} \sigma_{I_{L_i}} \sigma_{I_{L_j}} = \rho_{I_{L_i} I_{L_j}} \, \text{var}(I_L)$$

$$\overline{\left(I_{L_i} - \bar{I}_{L_i}\right)\left(I_{S_j} - \bar{I}_{S_j}\right)} = \rho_{I_{L_i} I_{S_j}} \sigma_{I_{L_i}} \sigma_{I_{S_j}} = \rho_{I_{L_i} I_{S_j}} \sigma_{I_L} \frac{\sigma_{I_L}}{\beta_m} = \rho_{I_{L_i} I_{L_j}} \frac{\text{var}}{\beta_m}(I_L)$$

$$\overline{\left(I_{S_i} - \bar{I}_{S_i}\right)\left(I_{S_j} - \bar{I}_{S_j}\right)} = \rho_{I_{S_i} I_{S_j}} \sigma_{I_{S_i}} \sigma_{I_{S_j}} = \rho_{I_{S_i} I_{S_j}} \frac{\text{var}\left(I_L\right)}{\beta_m^2}$$

The multi-look intensity image is

$$I_M = \alpha_L \sum_{i=1}^{L_L} I_{L_i} + \alpha_S \sum_{j=1}^{L_S} I_{Sj}$$

Thus, the mean value

$$\bar{I}_M = \alpha_L \overline{\sum_{i=1}^{L_L} I_{L_i}} + \alpha_S \overline{\sum_{j=1}^{L_S} I_{Sj}} = \alpha_L \sum_{i=1}^{L_L} \bar{I}_{L_i} + \alpha_S \sum_{j=1}^{L_S} \bar{I}_{Sj} = \alpha_L L_L \bar{I}_L + \alpha_S L_S \frac{\bar{I}_L}{\beta_m}$$

This mean value is chosen equal to the mean value of a large look.
Thus

$$\alpha_L L_L \bar{I}_L + \alpha_S L_S \frac{\bar{I}_L}{\beta_m} = \bar{I}_L$$

Hence

$$\alpha_L L_L + \frac{\alpha_S L_S}{\beta_m} = 1$$

The variance is obtained by

$$var(I_M) = \overline{\left(I_M - \bar{I}_M\right)^2} = \overline{\left\{ \alpha_L \sum_{i=1}^{L_L} \left(I_{L_i} - \bar{I}_{L_i}\right) + \alpha_S \sum_{j=1}^{L_S} \left(I_{Sj} - \bar{I}_{Sj}\right) \right\}^2}$$

$$= \alpha_L^2 \sum_{i=1}^{L_L} \sum_{j=1}^{L_L} \sigma_{I_{L_i}} \sigma_{I_{L_j}} \rho_{I_{L_i} I_{L_j}} + 2\alpha_L \alpha_S \sum_{i=1}^{L_L} \sum_{j=1}^{L_S} \sigma_{I_{L_i}} \sigma_{I_{Sj}} \rho_{I_{L_i} I_{Sj}} + \alpha_S^2 \sum_{i=1}^{L_S} \sum_{j=1}^{L_S} \sigma_{I_{S_i}} \sigma_{I_{Sj}} \rho_{I_{S_i} I_{Sj}}$$

$$= var(I_L) \left[\alpha_L^2 \sum_{i=1}^{L_L} \sum_{j=1}^{L_L} \rho_{I_{L_i} I_{L_j}} + \frac{2}{\beta_m} \alpha_L \alpha_S \sum_{i=1}^{L_L} \sum_{j=1}^{L_S} \rho_{I_{L_i} I_{Sj}} + \frac{\alpha_S^2}{\beta_m^2} \sum_{i=1}^{L_S} \sum_{j=1}^{L_S} \rho_{I_{S_i} I_{Sj}} \right]$$

Hence

$$ENL = \frac{1}{\left[\alpha_L^2 \sum_{i=1}^{L_L} \sum_{j=1}^{L_L} \rho_{I_{L_i} I_{L_j}} + \frac{2}{\beta_m} \alpha_L \alpha_S \sum_{i=1}^{L_L} \sum_{j=1}^{L_S} \rho_{I_{L_i} I_{Sj}} + \frac{\alpha_S^2}{\beta_m^2} \sum_{i=1}^{L_S} \sum_{j=1}^{L_S} \rho_{I_{S_i} I_{Sj}} \right]}$$

3.4.2 L_L overlapping large Hamming looks and 2 small rectangular looks

Figure 16 shows the positions of the various looks associated with this technique,
referred to as the HL7RS2 technique. Comparing with figure 12 in section 3.3.2
we see that the small Hamming weighted looks are replaced by small rectangular
ones. The expectation is that by using rectangular weighting functions for the
extreme looks rather than Hamming weighted ones we are able to improve the
radiometric resolution via the edge looks without having to sacrifice geometrical
resolution.
In section 3.3.2 we used edge looks with half the look size of the large ones. The
resolution of a rectangular look with this look size is better than the Hamming look
resolution but still worse than the resolution associated with the large Hamming
look. To obtain the same geometrical resolution we have to use a larger rectangular
look size. Below we consider two cases: one case where the resolution of an edge
look equals that of a large Hamming look and one where the look size of the edge
look is one half of that of a large look.

Note that by choosing the 3 dB resolution of the rectangular edge look equal to the resolution of the large Hamming look the sidelobe performance of the former is worse.
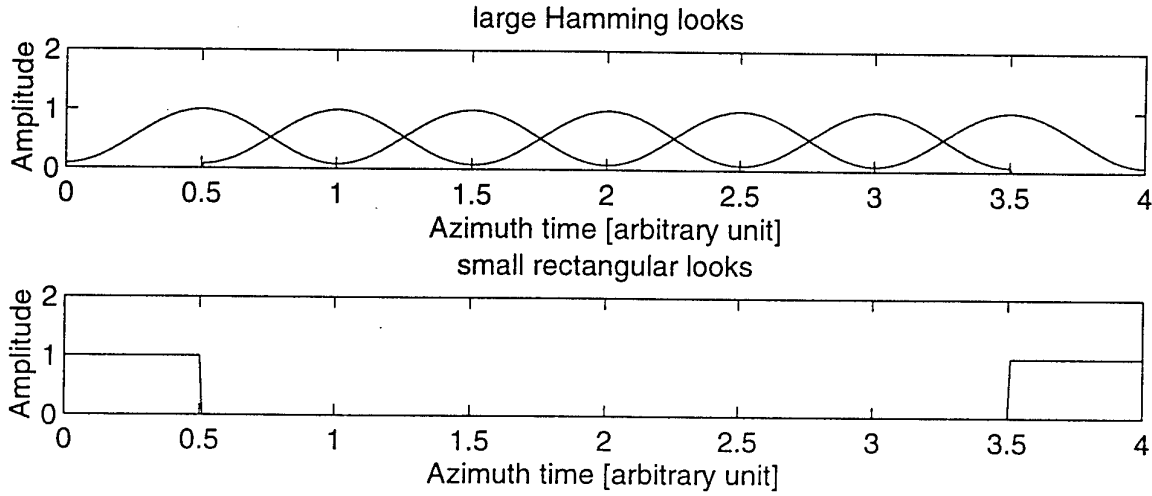

Figure 16:   Look configuration of the HL7RS2 multi-look technique.

As derived in section 3.4.1 we have

$$\bar{I}_m = \bar{I}_L$$

$$\alpha_L L_L + \frac{\alpha_S L_S}{\beta_m} = 1$$

$$ENL = \cfrac{1}{\alpha_L^2 \sum\limits_{i=1}^{L_L}\sum\limits_{j=1}^{L_L}\rho_{I_{L_i}I_{L_j}} + \cfrac{2}{\beta_m}\alpha_L\alpha_S\sum\limits_{i=1}^{L_L}\sum\limits_{j=1}^{L_S}\rho_{I_{L_i}I_{S_j}} + \cfrac{\alpha_S^2}{\beta_m^2}\sum\limits_{i=1}^{L_S}\sum\limits_{j=1}^{L_S}\rho_{I_{S_i}I_{S_j}}}$$

and

$$\beta_m = 0.3974\frac{T_H}{T_R}$$

As an example, we take an overlap of 50% for the large Hamming windows, the number of independent looks $L_i = 4$, $L_L = 2L_i-1$ and $L_S = 2$.
The figures 17 through 18a,b show the results where the resolution of the rectangular edge look is equal to the resolution of the large Hamming look. As derived in section 3.4.1 then $T_R = 0.685\, T_H$ and $\beta_m = 0.581$.

Figure 17 shows the ENL and 3 dB values as a function of α_S.
The maximum ENL value occurs for $\alpha_S = 0.0351$ and is equal to 6.70. This value is less than 7.6, the value obtained with Hamming edge looks. However, in the latter case the resolution is less, 1.38 compared to 1.31.
Compared to the IML technique we notice that the HL7RS2 technique offers a slight advantage in the low α_S range. The ENL values are almost equal but no

resolution is sacrificed. Also, the efficiency is higher, only 9 looks have to be computed compared with 22 in the IML case.
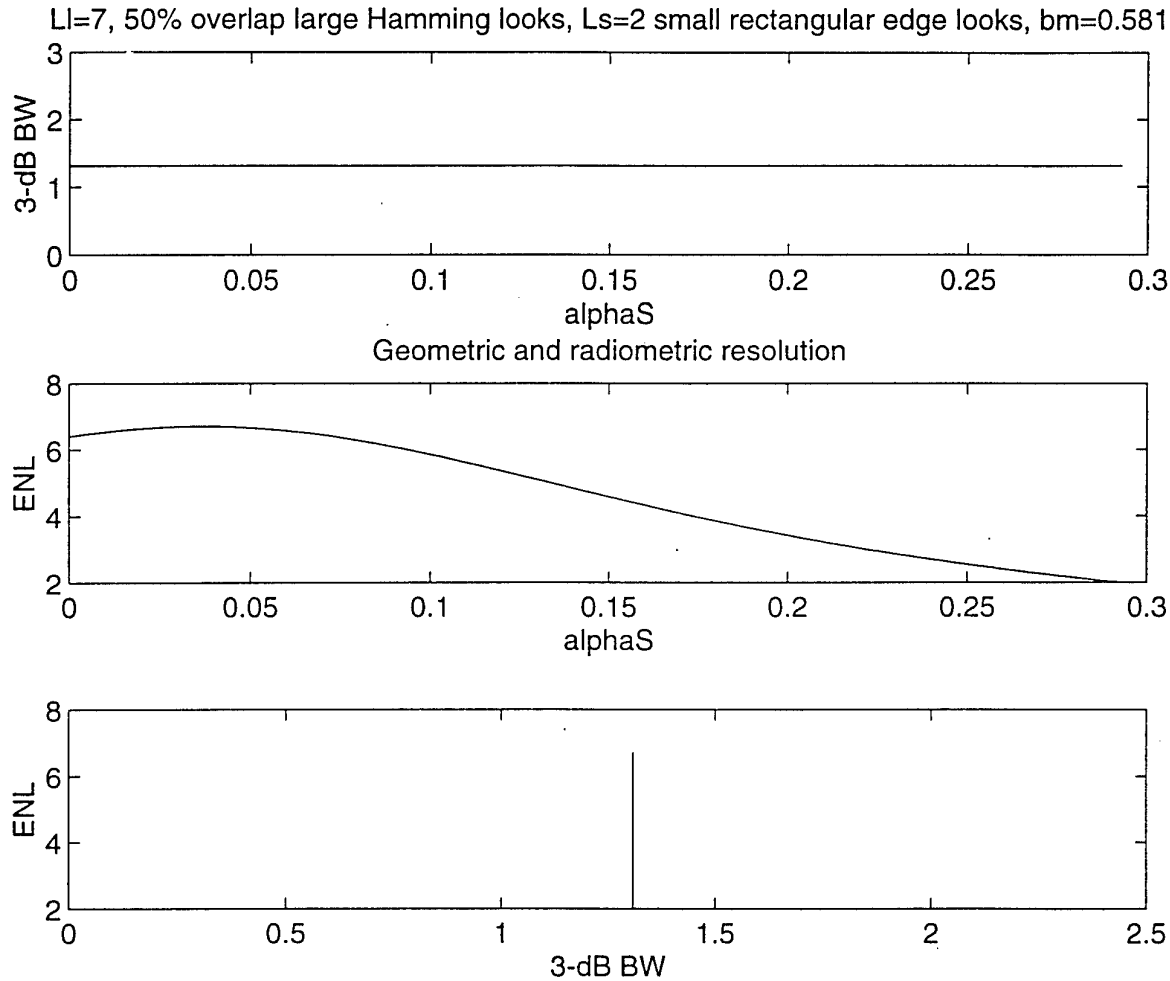

Figure 17:   The Equivalent Number of Looks and the 3 dB resolution as a function of α_S. All looks same resolution, $\beta_m = 0.581$.

Figures 18a and b show the azimuth impulse response of the HL7RS2 technique for three values of α_S. The value $\alpha_S = 0$ yields the result of a single look Hamming weighted image with $T_H = T_a/4$. The other extreme value ($\alpha_L = 0$) yields the result of a single look rectangular weighted image with $T_R = 0.685T_a/4$. The bottom curve shows the result for $\alpha_S = 0.0351$ which corresponds with the maximum ENL value attainable. Note that although the 3 dB resolution is equal to the resolution of the all Hamming case, the sidelobe character is worse due to the higher sidelobes of the rectangular look.

Figure 19 shows the result obtained with the HL7RS2 technique for $T_R = T_H/2$, $\beta_m = 0.795$. This figure can be compared with Figure 13, results from the HL7HS2 technique. In both figures we observe the α_S dependence of the resolution due to the inequality of the resolution of small and large looks. The HL7RS2 technique yields a maximum ENL value of 7.52 for $\alpha_S = 1.356$. The values for the HL7HS2

technique are ENL = 7.56 for α_S = 0.2. Thus the HL7RS2 technique yields a slightly smaller ENL value. However, the resolution is better, 3 dB value is 1.36 compared with 1.38, the HL7HS2 value.

Azimuth impulse response of multilook I=aL*sum of 7 looks IL + aS*sum of 2 looks IS

time arbitrary unit -> aL = 0.1429 aS = 0 3-dB BW = 1.31 / TL

time arbitrary unit -> aL = 0 aS = 0.2927 3-dB BW = 1.31 / TL

time arbitrary unit -> aL = 0.1257 aS = 0.0351 3-dB BW = 1.31 / TL
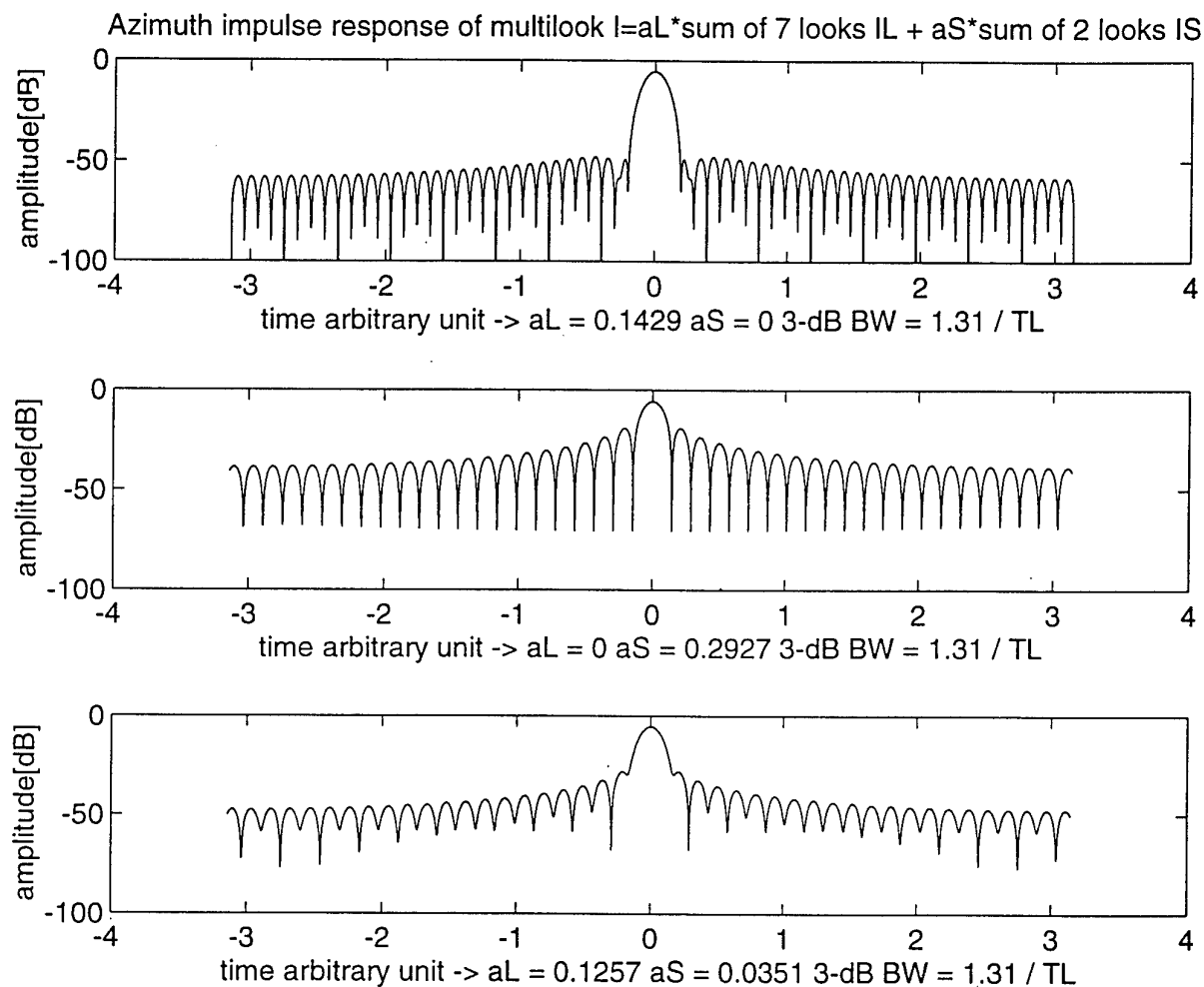
Figure 18a: Azimuth impulse response of the HL7RS2 multi-look technique for several values of α_S, logarithmic scale.

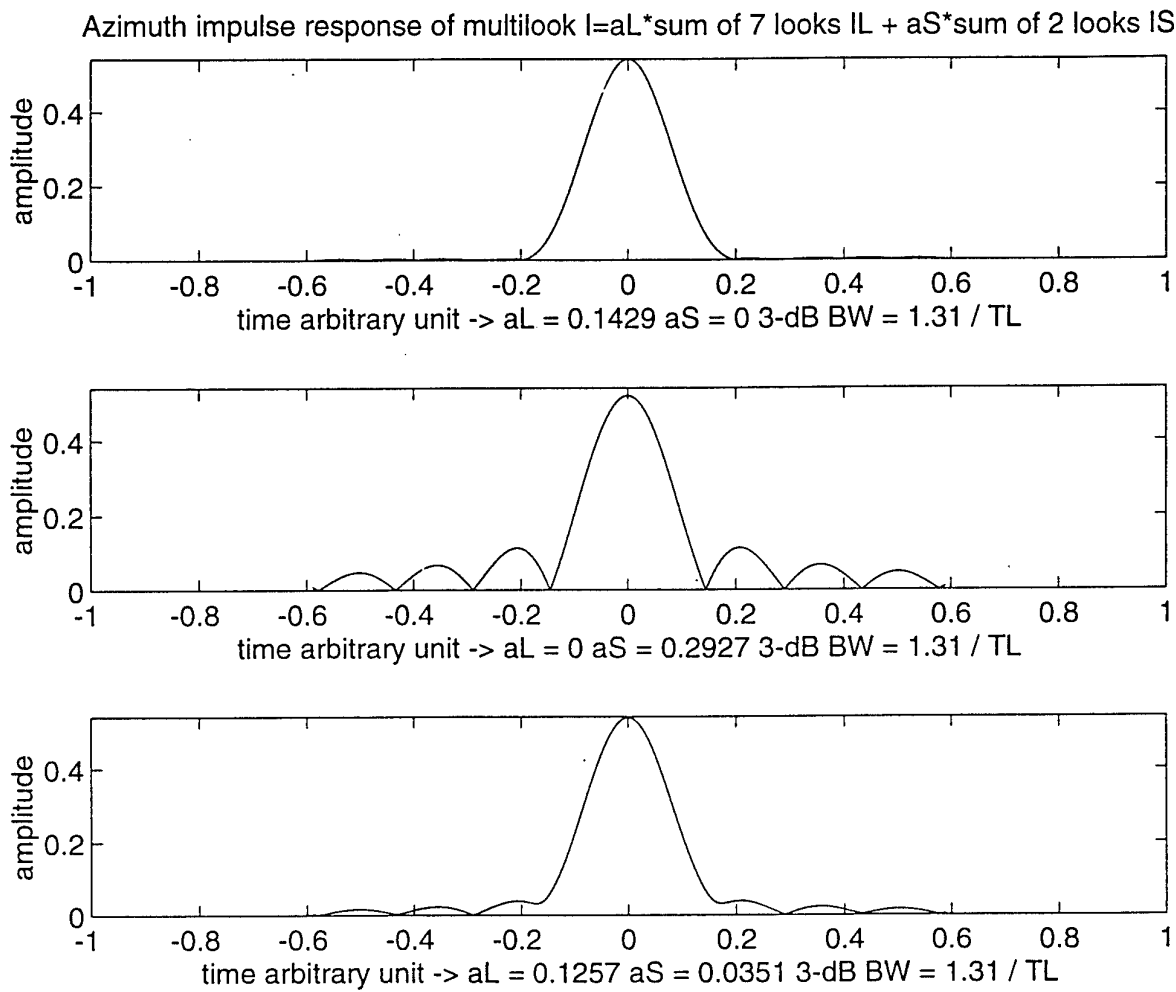*Figure 18b: Azimuth impulse response of the HL7RS2 multi-look technique for several values of α_S, linear scale.*

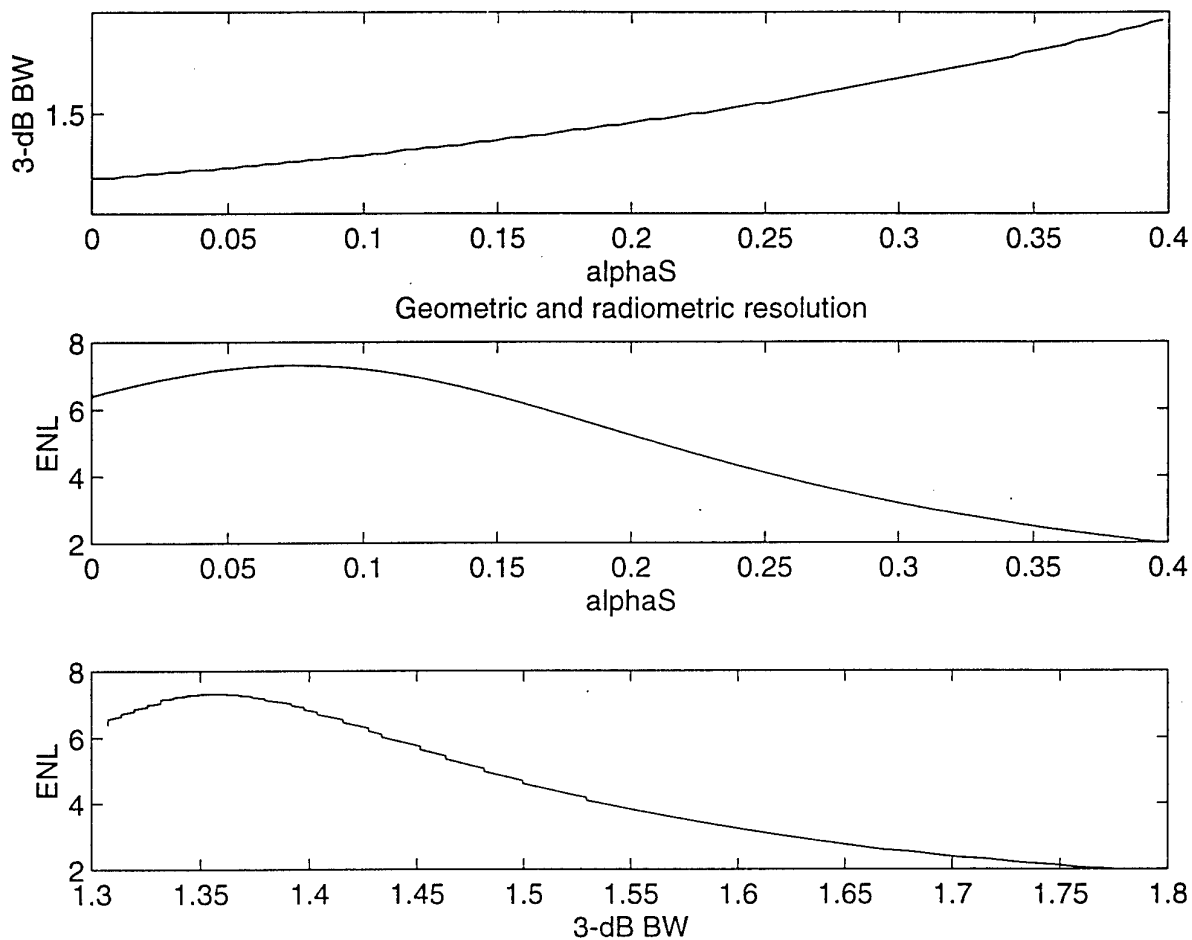LI=7, 50% overlap large Hamming looks, Ls=2 small rectangular edge looks, bm=0.795

Figure 19: The Equivalent Number of Looks and the 3 dB resolution as a function of α_S. $T_R = T_H/2$, $\beta_m = 0.795$.

3.5   Visual illustrations of multi-look techniques

The results of various multi-look techniques are shown in the form of the images
R2, R3 and R4. The techniques have been implemented in the Generic SAR
Processor (GSP) of TNO-FEL. The GSP is a software package that runs on a SUN
workstation and is able to process both airborne and satellite SAR data. The raw
SAR input data is part of raw image data of the ERS1 satellite SAR. The scene
consists of the entrance to the port of Rotterdam and part of its environment. A
map of the area is shown by R1.
Output of the processor are 7 single-look images (L0, L1, L2, L3, L4, L5 and L6).
The images have 50% overlap. Hamming weighting is used. The slant range
resolution is 9 m and the azimuth resolution is 32 m.
Image R2 shows the central single-look image L3. The speckle noise is clearly
visible, masking weak details and interrupting line structures. The interruption
occurs as a low speckle value is realised.
Image R3 shows the multi-look image consisting of the combination of the 4 non
overlapping looks: L0, L2, L4 and L6. The corresponding equivalent number of
looks ENL = 4. The speckle reduction, compared to R2, is clearly visible, more
weak details emerge and very few line structures are interrupted. The probability
of occurrence of a low speckle value in each of the four images is low.
Image R4 shows the multi-look image consisting of the combination of all 7
single-look images, L0 through L6. The corresponding equivalent number of looks
is ENL = 6.4. Again an improvement can be observed albeit less than going from
R2 to R3.
Some remarks are in order. First, visual quality is higher on a monitor, some is lost
by the copying process. Second, speckle reduction is advantageous to both men
and machine. A human interpretor sees more weak details. A computer algorithm
can use the improved signal-to-noise ratio to perform better. Degrees of speckle
reduction insignificant to man can still be useful for very demanding applications.
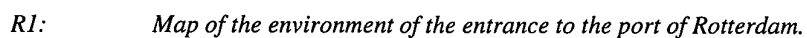
R1:   *Map of the environment of the entrance to the port of Rotterdam.*

R2. *Single look of L4 independent looks.*

R3:   Multi-look image, combination of 4 independent looks.

R4: Multi-look image, combination of 7 overlapping looks.

4. The azimuth impulse response

In order to assess a multi-look technique two values are important: the Equivalent Number of Looks (ENL) and the resolution measured by the 3 dB width of the main lobe (BW) of the azimuth impulse response. The impulse response of the multi-look technique is a weighted sum of the responses of the large and small looks.

$$I_M = \alpha_L \sum_{i=1}^{L_L} I_{L_i} + \alpha_S \sum_{j=1}^{L_S} I_{S_j}$$

The main lobe width BW is determined via an iterative procedure. For an accurate result a densely sampled impulse response I_M is required. If the constituent response sequences I_L and I_S are given in formula form, the samples are readily computed. In this report only the rectangular and Hamming weighting functions are considered and the corresponding response functions are analytically known, at least the main lobe part. So, we have used the known formulae. If these formulae were not known, a numerically obtained response sequence must be used. In this case the sequence must be heavily interpolated to yield a result which can be used for a sufficiently accurate BW value.

In the report a number of azimuth impulse responses are shown. The main lobe of these curves were used to determine the BW value. Use of the analytical description of the main lobe is correct, however, the description is not correct for the sidelobes [ref. 5, section 7.6]. The derived formulae are based on the assumption that the linear FM spectrum has a rectangular amplitude distribution. The amplitude ripple of the actual spectrum can be related to the existence of distortion sidelobes that can be considerably greater than the -40 dB level that can be obtained by the Hamming weighting (see Figure 7.22 in ref. 5).

The Figures 20a and 20b show the azimuth impulse responses of the HL7HS2 multi-look technique. These curves were obtained by computer simulation (digitally computed cross correlation sequence). Comparing these figures with the ones shown by the figures 15a and b, which are based on the analytical description of the main lobe, we see a marked difference in sidelobe behaviour.

The computer simulated curves were obtained by using the ERS-1 satellite parameters. The full resolution azimuth response uses a bandwidth of Ba = 1300 Hz and an integration time of T_a = 0.6 sec, yielding a bandwidth time product of about 800.

The spectrum corresponding to such a high BT product shows fairly well a rectangular amplitude distribution and a very good sidelobe behaviour (not shown here). However, the large and small looks have BT products which are much lower. For instance, the small look spans Ta/8 seconds. The azimuth frequency rate is $\dfrac{B_a}{T_a}$ thus, the look has a BT product of only $\dfrac{T_a}{8} \cdot \dfrac{B_a}{T_a} \cdot \dfrac{T_a}{8} = \dfrac{B_a T_a}{64} = 12 .5$

Therefore, the spectrum is far from rectangular and a decreased sidelobe character can be expected.

Thus, we conclude that the shown azimuth impulse responses must be interpreted
with care, the main lobe part is correct, however, the sidelobe behaviour is too
optimistic.

Azimuth impulse response of multilook I=aL*sum of 7 looks IL + aS*sum of 2 looks IS
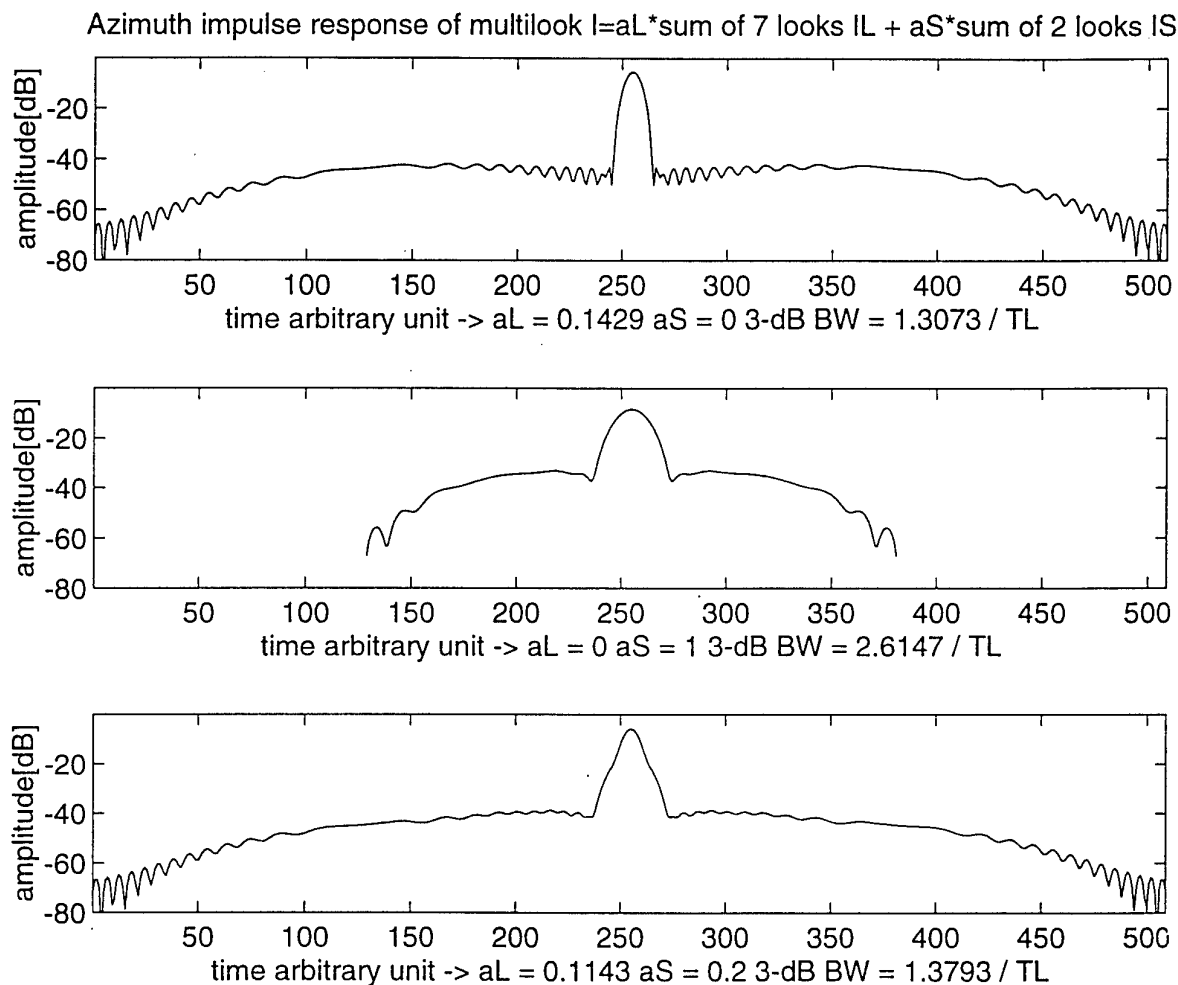
Figure 20a: *Azimuth impulse response of the HL7RS2 multi-look technique for several values of α_S, logarithmic*
scale.

Azimuth impulse response of multilook I=aL*sum of 7 looks IL + aS*sum of 2 looks IS

time arbitrary unit -> aL = 0.1429 aS = 0 3-dB BW = 1.3073 / TL

time arbitrary unit -> aL = 0 aS = 1 3-dB BW = 2.6147 / TL

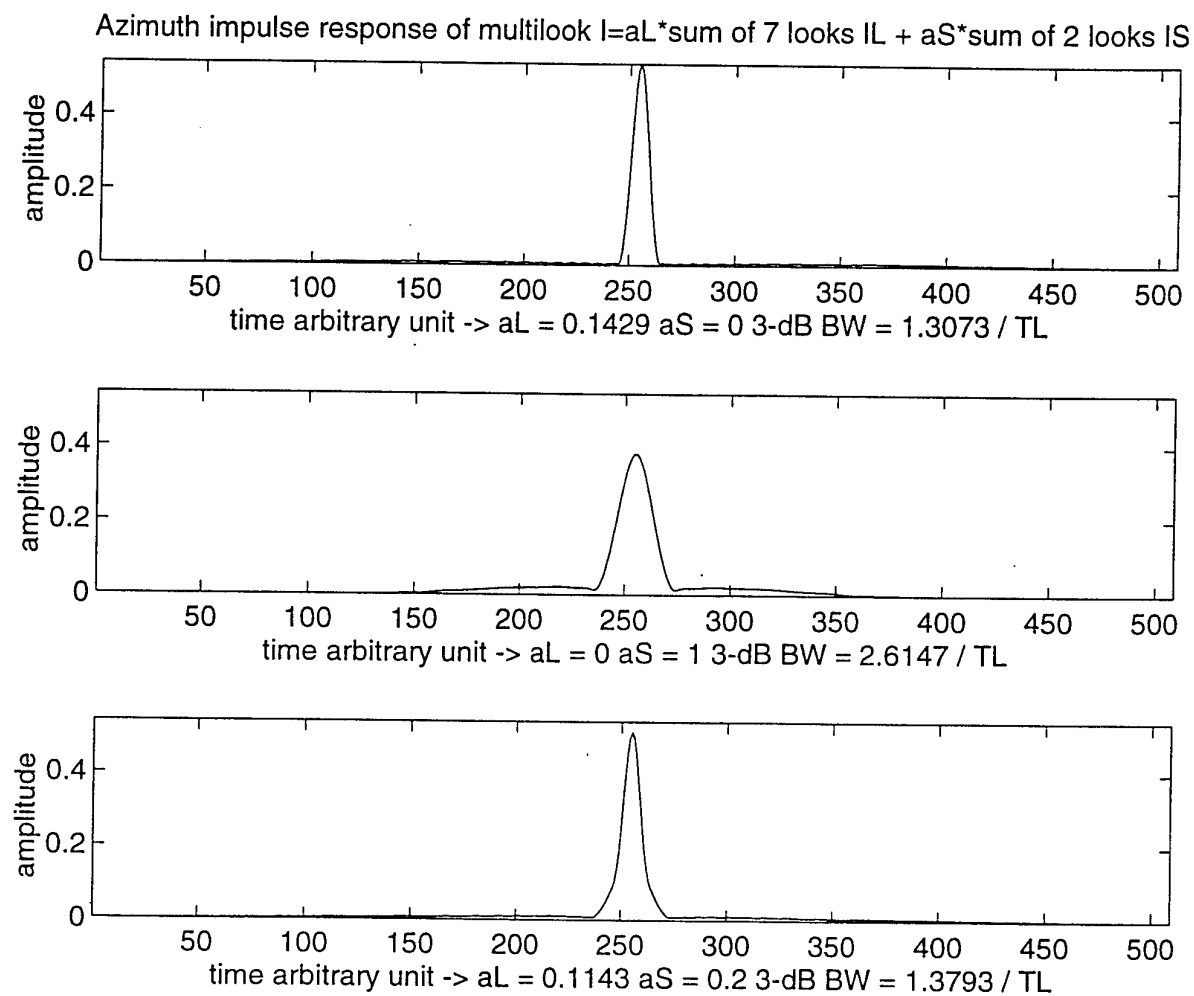time arbitrary unit -> aL = 0.1143 aS = 0.2 3-dB BW = 1.3793 / TL

Figure 20b: Azimuth impulse response of the HL7RS2 multi-look technique for several values of α_S, linear scale.

5.   Conclusions

We have evaluated the effects on SAR imagery of a number of different speckle
reduction techniques. Each technique uses a number of single look intensity
images of which the weighted sum, the multi-look image is formed. The
constituent single looks differ in size T (B) and weighting function used. It is
shown that the speckle behaviour of each look is the same and that they differ in
geometric resolution, i.e. the width of the main lobe of the impulse response.
Since, the lower geometric resolution looks do not make efficient use of the signal
energy, speckle reduction can be obtained, increase in the ENL's, by multi-look
technique. By using overlapping looks, a more efficient use is made of the
available bandwidth.
We have evaluated three types of techniques: techniques using equal looks with a
rectangular weighting function, techniques that use equal looks with a Hamming
weighting function, and techniques that use two kinds of weighting function sizes.
It has been shown that the last techniques are able to fill the left and right
extremities of the signal bandwidth by positioning there small looks. However, the
general pattern, trading geometric resolution for radiometric resolution, holds,
since the smaller looks have a lower geometric resolution. The IML technique
forms the multi-look image by computing the weighted sum of the large and small
looks. By varying the factor α_S continuously a continuous trading of geometric and
radiometric resolution is obtained.
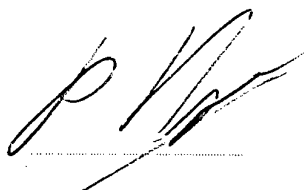
As a measure of geometric resolution, the 3-dB width of the main lobe of the
impulse response is used. However, two responses can have the same 3-dB value
and differ in detailed main lobe and sidelobe structures. The effects of different
impulse response shapes on image interpretation may be important.
We have analysed the techniques assuming a flat azimuth spectrum. The effects of
the shape of the spectrum can be analysed for each individual system and a more
realistic value of the ENL can be calculated. A potential drawback of the multi-
look techniques yielding improved ENL values is that many more looks have to be
computed. However, there may be cases where the utmost attainable ENL value is
a necessity.

6.   References

[1] A. Moreira, 'An Improved Multi-look Technique to Produce SAR Imagery',
    Proceedings IEEE International Radar Conference 1990.
[2] F. K. Li, C. Croft, and D. N. Held, 'Comparison of Several Techniques to
    Obtain Multiple-look SAR Imagery', IEEE Transactions on Geoscience and
    Remote Sensing, Vol. GE-21, No. 3, July 1983.
[3] F. J. Harris, 'On the Use of Windows for Harmonic Analysis with the Discrete
    Fourier Transform', Proceedings of the IEEE, Vol. 66, No. 1, January 1978.
[4] A.Papoulis, 'Probability, Random variables, and Stochastic Processes',
    McGraw-Hill Book Company.
[5] C.E. Cook and M. Bernfeld, 'Radar Signals, an introduction to theory and
    application', Academic Press.

7. Signature

P. Hoogeboom
Group leader

F.P.Ph. de Vries
Author

Appendix A   The correlation coefficients ρ_{xy} and $\rho_{I_x I_y}$

A.1   The correlation coefficient ρ_{xy} of two complex valued single look images

Pc(f)

Pc

```
<----------------------- Available bandwidth Ba  ------------------>
```
0   --> f
                                                                                       PRF

exp(j phi(ta))

```
<----------------------- Available integration time Ta  ------------------>
```
-Ta/2   Ta/2   --> ta

w(ta)

weighting functions wx(ta) and wy(ta)

-Ta/2   Ta/2   --> ta
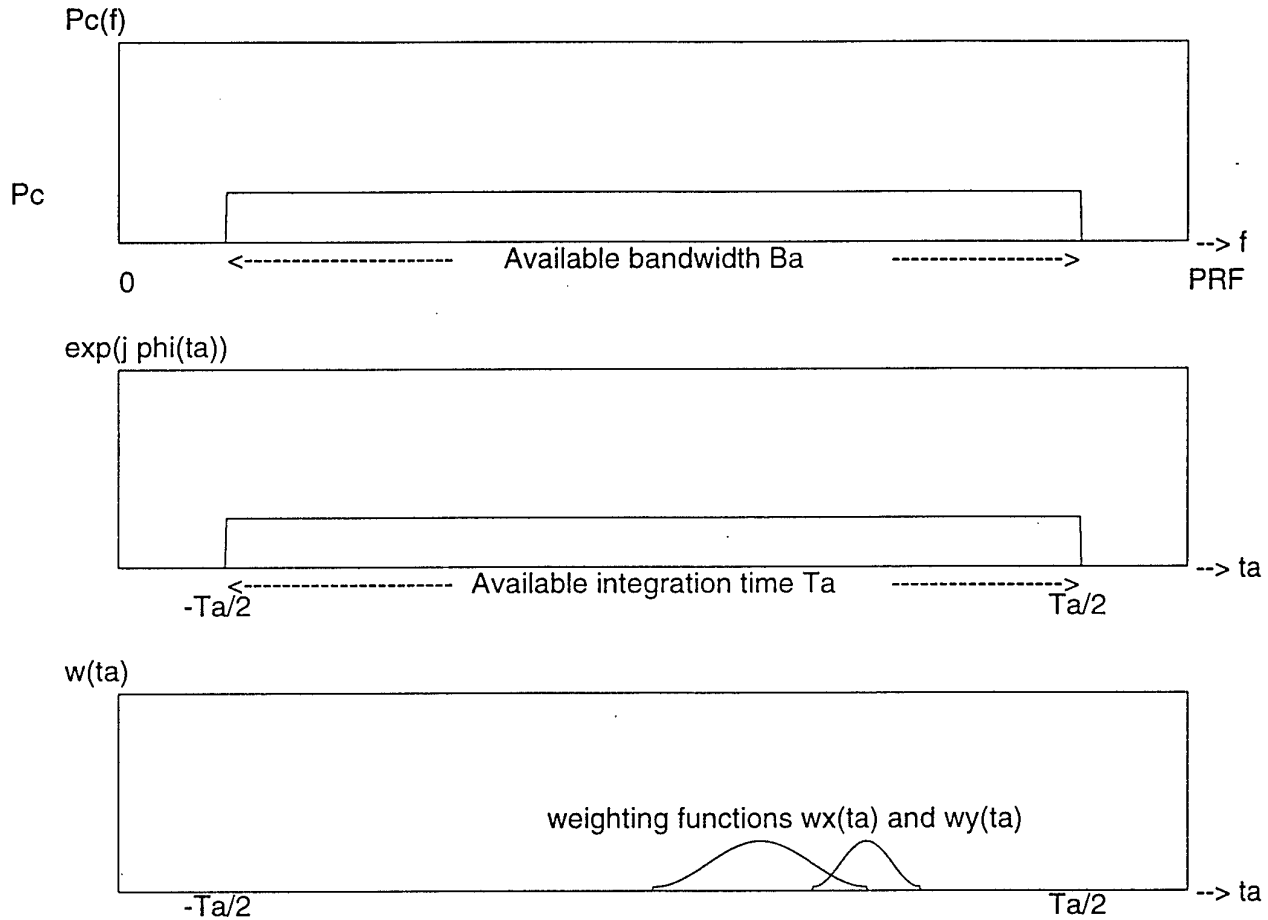
Figure A.1:   Available SAR spectrum, reference function and position of two overlapping looks.

The cross spectral density of two complex single look images is

$$P_{xy}(f) = H_x(f) H_y^*(f) P_c(f)$$

where $H_x(f)$ and $H_y(f)$ are the frequency transfer functions of the x and y outputs respectively, and $P_c(f)$ is the azimuth clutter power density spectrum.

The cross-covariance $\mu_{xy} = \overline{(x - \bar{x})(y - \bar{y})^*}$ is given by

$$\mu_{xy} = R_{xy}(0) = \int P_{xy}(f) df = P_c \int H_x(f) H_y^*(f) df = P_c \int h_x(t) h_y^*(t) dt$$

The azimuth reference function is

$$h(t) = \varepsilon^{j\varphi(t)} \qquad -T_a/2 \le t \le T_a/2$$

Hence the look reference functions are

$$h_x(t) = w_x(t - t_{c_x})h(t) \qquad t_{c_x} - T_x/2 \le t \le t_{c_x} + T_x/2$$

$$h_y(t) = w_y(t - t_{c_y})h(t) \qquad t_{c_y} - T_y/2 \le t \le t_{c_y} + T_y/2$$

where $w_x(\ )$ and $w_y(\ )$ are the (real) window functions. Substitution gives

$$\mu_{xy} = P_c \int w_x(t - t_{cx})h(t)w_y(t - t_{cy})h^*(t)dt$$

$$\mu_{xy} = P_c \int w_x(t - t_{cx})w_y(t - t_{cy})dt$$

Without loss of generality we take $T_x \ge T_y$ and $t_x = 0$. Thus

$$\mu_{xy} = P_c \int w_x(t)w_y(t - t_{c_y})dt$$

The variance of x and y are

$$var(x) = \overline{(x - \bar{x})(x - \bar{x})^*} = P_c \int w_x^2(t)dt$$

$$var(y) = \overline{(y - \bar{y})(y - \bar{y})^*} = P_c \int w_y^2(t)dt$$

Hence, the correlation coefficient $\rho_{xy} = \dfrac{\mu_{xy}}{\sigma_x \sigma_y}$ is

$$\rho_{xy} = \frac{\int w_x(t)w_y(t - t_{cy})dt}{\sqrt{\int w_x^2(t)dt}\sqrt{\int w_y^2(t)dt}}$$

A.2 The correlation coefficient $\rho_{I_x I_y}$ of two intensity images

The statistics of the real and imaginary part of the complex valued images x and y are

$$\overline{x_r} = \overline{x_i} = 0$$

$$\overline{x_r x_i} = 0$$

$$\mathrm{var}(x_r) = \mathrm{var}(x_i) = \sigma_x^2$$

$$\overline{y_r} = \overline{y_i} = 0$$

$$\overline{y_r y_i} = 0$$

$$\mathrm{var}(y_r) = \mathrm{var}(y_i) = \sigma_y^2$$

$$\overline{x_r y_r} = \overline{x_i y_i}$$

$$\overline{x_r y_i} = -\overline{x_i y_r}$$

The stochastic variables x_r, x_i, y_r and y_i have a Gaussian probability density function. Thus the intensity has an exponential pdf with

$$I_x = 2\sigma_x^2$$

$$\mathrm{var}(I_x) = I_x^2 = 4\sigma_x^4$$

Thus, the statistics of the complex valued images are

$$\overline{x} = \overline{x_r + jx_i} = 0$$

$$\mathrm{var}(x) = \overline{(x - \overline{x})(x - \overline{x})^*} = \overline{xx^*} = \overline{x_r^2} + \overline{x_i^2} = 2\sigma_x^2$$

$$\overline{y} = \overline{y_r + jy_i} = 0$$

$$\mathrm{var}(y) = \overline{(y - \overline{y})(y - \overline{y})^*} = \overline{yy^*} = \overline{y_r^2} + \overline{y_i^2} = 2\sigma_y^2$$

$$\mu_{xy} = \overline{(x - \overline{x})(y - \overline{y})^*} = \overline{xy^*} = \overline{x_r y_r} + \overline{x_i y_i} + j\left(\overline{x_i y_r} - \overline{x_r y_i}\right) = 2\left(\overline{x_r y_r} + j\overline{x_i y_r}\right)$$

The correlation coefficient between x and y is given by

$$\rho_{xy} = \frac{\mu_{xy}}{\sqrt{\mathrm{var}(x)}\sqrt{\mathrm{var}(y)}} = \frac{\overline{x_r y_r} + j\overline{x_i y_r}}{\sigma_x \sigma_y}$$

Hence

$$|\rho_{xy}|^2 = \frac{\overline{x_r y_r}^2 + \overline{x_i y_r}^2}{\sigma_x^2 \sigma_y^2}$$

The real valued intensity images are

$$I_x = x_r^2 + x_i^2$$

$$I_y = y_r^2 + y_i^2$$

Thus, the statistics of the intensity images are

$$\bar{I}_x = \overline{x_r^2} + \overline{x_i^2} = 2\sigma_x^2$$

$$\bar{I}_y = \overline{y_r^2} + \overline{y_i^2} = 2\sigma_y^2$$

$$\text{var}(I_x) = \overline{\left(I_x - \bar{I}_x\right)^2} = 4\sigma_x^4$$

$$\text{var}(I_y) = \overline{\left(I_y - \bar{I}_y\right)^2} = 4\sigma_y^4$$

The cross-covariance is

$$\mu_{I_x I_y} = \overline{\left(I_x - \bar{I}_x\right)\left(I_y - \bar{I}_y\right)} = \overline{I_x I_y} - \bar{I}_x \bar{I}_y = \overline{I_x I_y} - 4\sigma_x^2 \sigma_y^2$$

$$\overline{I_x I_y} = \overline{\left(x_r^2 + x_i^2\right)\left(y_r^2 + y_i^2\right)} = \overline{x_r^2 y_r^2} + \overline{x_r^2 y_i^2} + \overline{x_i^2 y_r^2} + \overline{x_i^2 y_i^2}$$

Since x_r and y_r are Gaussian

$$\overline{x_r^2 y_r^2} = \bar{x}_r^2 \bar{y}_r^2 + 2\overline{x_r y_r}^2$$

Substitution yields

$$\overline{I_x I_y} = 4\left(\overline{x_r y_r}^2 + \overline{x_i y_r}^2\right)$$

Thus

$$\rho_{I_x I_y} = \frac{\mu_{I_x I_y}}{\sqrt{\text{var}(I_x)}\sqrt{\text{var}(Iy)}} = \frac{\overline{x_r y_r}^2 + \overline{x_i y_r}^2}{\sigma_x^2 \sigma_y^2}$$

Hence

$$\rho_{I_x I_y} = \left|\rho_{xy}\right|^2$$

The correlation coefficient of the intensity images is equal to the modules squared of the correlation coefficient of the complex images.

REPORT DOCUMENTATION PAGE
(MOD-NL)

1. DEFENCE REPORT NO (MOD-NL)	2. RECIPIENT'S ACCESSION NO	3. PERFORMING ORGANIZATION REPORT NO
TD97-0122		FEL-96-A015

4. PROJECT/TASK/WORK UNIT NO	5. CONTRACT NO	6. REPORT DATE
24923	A93KM727	January 1998

7. NUMBER OF PAGES	8. NUMBER OF REFERENCES	9. TYPE OF REPORT AND DATES COVERED
47 (incl 1 appendix, excl RDP & distribution list)	5	

10. TITLE AND SUBTITLE

Speckle reduction in SAR Imagery by various multi-look techniques

11. AUTHOR(S)

F.P.Ph. de Vries

12. PERFORMING ORGANIZATION NAME(S) AND ADDRESS(ES)

TNO Physics and Electronics Laboratory, PO Box 96864, 2509 JG The Hague, The Netherlands
Oude Waalsdorperweg 63, The Hague, The Netherlands

13. SPONSORING AGENCY NAME(S) AND ADDRESS(ES)

Royal Netherlands Navy
Van der Burchlaan 31, 2597 PC The Hague, The Netherlands

14. SUPPLEMENTARY NOTES

The classification designation Ongerubriceerd is equivalent to Unclassified, Stg. Confidentieel is equivalent to Confidential and Stg. Geheim is equivalent to Secret.

15. ABSTRACT (MAXIMUM 200 WORDS (1044 BYTE))

SAR images are contaminated by speckle noise. Multi-look imaging is used for its alleviation. In this report, we discuss the performance of several techniques to generate multi-look images. It is shown that the geometric resolution of the impulse response can be traded for the radiometric resolution. The various techniques differ in the use of single looks, number, size and weighting function. It is found that by properly positioning of overlapping looks in the spectral domain, the equivalent number of looks is substantially higher than the number of independent looks.

16. DESCRIPTORS	IDENTIFIERS
Multiple-look SAR imagery Speckle Speckle reduction techniques	Synthetic aperture radar Signal processing Image enhancement

17a. SECURITY CLASSIFICATION (OF REPORT)	17b. SECURITY CLASSIFICATION (OF PAGE)	17c. SECURITY CLASSIFICATION (OF ABSTRACT)
Ongerubriceerd	Ongerubriceerd	Ongerubriceerd

18. DISTRIBUTION AVAILABILITY STATEMENT		17d. SECURITY CLASSIFICATION (OF TITLES)
Unlimited Distribution		Ongerubriceerd

Distributielijst

1.	DWOO
2.	HWO-KM
3.	HWO-KL*
4.	HWO-KLu*
5.	HWO-CO*
6.	KM/Dienst Hydrografie, t.a.v. KTZ L. ter Haar
7.	DM&P TNO-DO
8.	Directie TNO-PML*
9.	Directie TNO-TM*
10 t/m 12.	Bibliotheek KMA
13.	DMKM/WCS/COSPON, t.a.v. Drs. W. Pelt
14.	MARSTAF/OBS/OB, t.a.v. LTZ1 Ir. J. Franken
15.	DMKM/WCS/EMDC, t.a.v. Ing. H. Quik
16.	DS/CZ-D, t.a.v. Ir. J.B.J. Orbons
17.	DMKLu/MWFAA, t.a.v. Maj. Ir. R. Thaens
18.	DMKLu, t.a.v. Ir. S.J.J. de Bruin
19.	DOPKLu/STAORE, t.a.v. Maj. Ir. T.W.G. de Laat
20.	DMKL, t.a.v. Ing. A.J. Kramps
21.	Directie TNO-FEL, t.a.v. Dr. J.W. Maas
22.	Directie TNO-FEL, t.a.v. Ir. J.A. Vogel, daarna reserve
23.	Archief TNO-FEL, in bruikleen aan MPC*
24.	Archief TNO-FEL, in bruikleen aan Ir. C. Eberwijn
25.	Archief TNO-FEL, in bruikleen aan Ir. P. Hoogeboom
26.	Archief TNO-FEL, in bruikleen aan Dr. H.S.F. Greidanus
27.	Archief TNO-FEL, in bruikleen aan Ir. J.C.M. Kleijweg
28.	Archief TNO-FEL, in bruikleen aan Drs. J.H. Aardoom
29.	Archief TNO-FEL, in bruikleen aan Ing. R.J. Dekker
30.	Archief TNO-FEL, in bruikleen aan Ir. M.P.G. Otten
31.	Archief TNO-FEL, in bruikleen aan Dr. A.C. van den Broek
32.	Archief TNO-FEL, in bruikleen aan Ir. F.P.Ph. de Vries
33.	Documentatie TNO-FEL
34.	Reserve

Indien binnen de krijgsmacht extra exemplaren van dit rapport worden gewenst door personen of instanties die niet op de verzendlijst voorkomen, dan dienen deze aangevraagd te worden bij het betreffende Hoofd Wetenschappelijk Onderzoek of, indien het een K-opdracht betreft, bij de Directeur Wetenschappelijk Onderzoek en Ontwikkeling.

* Beperkt rapport (titelblad, managementuittreksel, RDP en distributielijst).